Available online at www.sciencedirect.com
SCIENCE DIRECT®
ELSEVIER
International Journal of Solids and Structures 42 (2005) 5274–5306
INTERNATIONAL JOURNAL OF SOLIDS and STRUCTURES
www.elsevier.com/locate/ijsolstr

Nonlinear analysis of a composite panel with a cutout repaired by a bonded tapered composite patch

E. Oterkus [a], A. Barut [a], E. Madenci [a,*], D.R. Ambur [b]

[a] *Aerospace and Mechanical Engineering, The University of Arizona, Tucson, AZ 85721, United States*
[b] *NASA Langley Research Center, Hampton, VA 23681, United States*

Received 2 March 2004; received in revised form 15 February 2005
Available online 29 March 2005

Abstract

This study presents a solution method to analyze the geometrically nonlinear response of a patch-repaired flat panel (skin) with a cutout under general loading conditions. The effect of induced stiffening due to tensile loading on the in-plane and, particularly, the out-of-plane behaviors of the patch-repaired skin are investigated. The damage to the skin is represented in the form of a cutout under the patch. The patch with tapered edges is free of external tractions. The skin is subjected to general boundary and loading conditions along its external edge. The solution method provides the transverse shear and normal stresses in the adhesive between the skin and the patch, and in-plane and bending stresses in the patch and skin. Both the patch and skin are made of linearly elastic composite laminates, and the adhesive between them is homogeneous and isotropic, exhibiting a bi-linear elastic behavior. Modified Green's strain–displacement relations in conjunction with von Karman assumptions are employed in determining the in-plane strains in the skin and patch; however, the transverse shear strains in the adhesive are determined based on the shear-lag theory. The present solution method utilizes the principle of virtual work in conjunction with complex potential functions.

1. Introduction

The objectives of a patch repair are to restore the static strength and durability of a structure and to decrease stress concentrations caused by damage in the form of a circular or an elliptical cutout. An essential part of the repair design is the prediction of the strength of the patch-repair and its effectiveness in reducing the stress concentrations around the cutout. The strength of a bonded patch repair depends on the surface preparation, geometries of the patch and damage area, material properties, and the adhesive

* Corresponding author. Tel.: +1 520 621 6113; fax: +1 520 621 8191.
E-mail address: madenci@email.arizona.edu (E. Madenci).

0020-7683/$ - see front matter © 2005 Elsevier Ltd. All rights reserved.
doi:10.1016/j.ijsolstr.2005.02.024

thickness and its possible variation and exposure to adverse environments. Furthermore, reduction of the transverse and peel stress concentrations along the edges of the adhesive is important in order to prevent premature failure of the bonded repair. Peak transverse shear stresses in the adhesive can be reduced by tapering the patch thickness near its edges.

A majority of the previous analytical investigations on the analysis of bonded patch repair of composite skin are based on the small deflection theory, in which the strain measure does not include the higher-order displacement terms. However, under uniaxial loading, the bending stiffness of both the patch and skin increases due to the induced stiffness arising from tensile loading, thus affecting the bending deformation significantly. This stiffening effect can only be included by considering the nonlinear (higher-order) displacement terms in the strain measure. Although there are only a few, recent investigations on bonded patch repair analysis include the effect of geometric nonlinearity (Klug and Sun, 1998; Naboulsi and Mall, 1998; Andruet et al., 2001; Tong and Xiannian, 2003; Duong and Yu, 2003). In most of these studies, either a commercially available finite element program is utilized (Klug and Sun, 1998), or special finite element models are developed based on two-dimensional elements (Naboulsi and Mall, 1998), or combined two- and three-dimensional elements with appropriate constraint conditions between the adhesive and adherents are used (Andruet et al., 2001; Tong and Xiannian, 2003).

In finite element analysis, the adhesive requires a highly refined three-dimensional mesh in order to keep the proper aspect ratio between the elements in adherends and adhesives. In the case of geometric and material nonlinearities, the iterative solution of the governing equations in which the global stiffness matrix is repeatedly calculated, the three-dimensional finite element analysis of the entire domain becomes computationally demanding. Therefore, both global and local models become necessary as performed by Barut et al. (2002) to capture acceptable accuracy. Thus, it is beneficial to have an efficient special-purpose analysis method that can be used to conduct extensive parametric studies in a timely manner and at relatively low computational costs. An analytic study was also performed for the geometrically nonlinear analysis of bonded patch repairs of infinitely long skin with a crack (Duong and Yu, 2003) for which the adhesive is assumed to be rigid, thus excluding the deformation in the adhesive. In all of these patch-repair studies, an untapered patch is bonded over a crack that represents the damage rather than a cutout.

This study extends the approach by Barut et al. (2002) to address the geometrically nonlinear behavior of a composite skin with a cutout repaired by bonding a tapered composite patch. In particular, it investigates the effects of stress stiffening, thickness of the tapered patch, and the patch lamination, as well as the bi-linear elastic behavior of the adhesive on the in-plane stresses in the skin and patch and the transverse normal and transverse shear stresses in the adhesive. The tapered patch thickness becomes especially important in reducing the stress concentrations near the adhesive edges. The isotropic adhesive exhibits either a linear elastic or a bi-linear elastic behavior. The damage to the skin is represented in the form of a circular cutout.

The nonlinear governing equations are derived based on the principal of virtual work in conjunction with a Rayleigh–Ritz semi-analytical solution method. In order to demonstrate the capabilities of the present analysis method, two patch-repair configurations are considered for the numerical results. The first problem investigates the effect of a tapered aluminum patch bonded over a circular cutout in an aluminum skin having a linear elastic adhesive material behavior. The second problem investigates the effect of a bi-linear elastic adhesive behavior on the repair of a composite skin having a circular cutout with an untapered composite patch.

2. Problem statement

The patch-repair configuration shown in Fig. 1 consists of a composite patch bonded to the skin with a circular or an elliptical hole representing the damage. The adhesive thickness is uniform. The elliptical cutout, which can be located arbitrarily in the skin under the patch, has a semi-major axis and a semi-minor

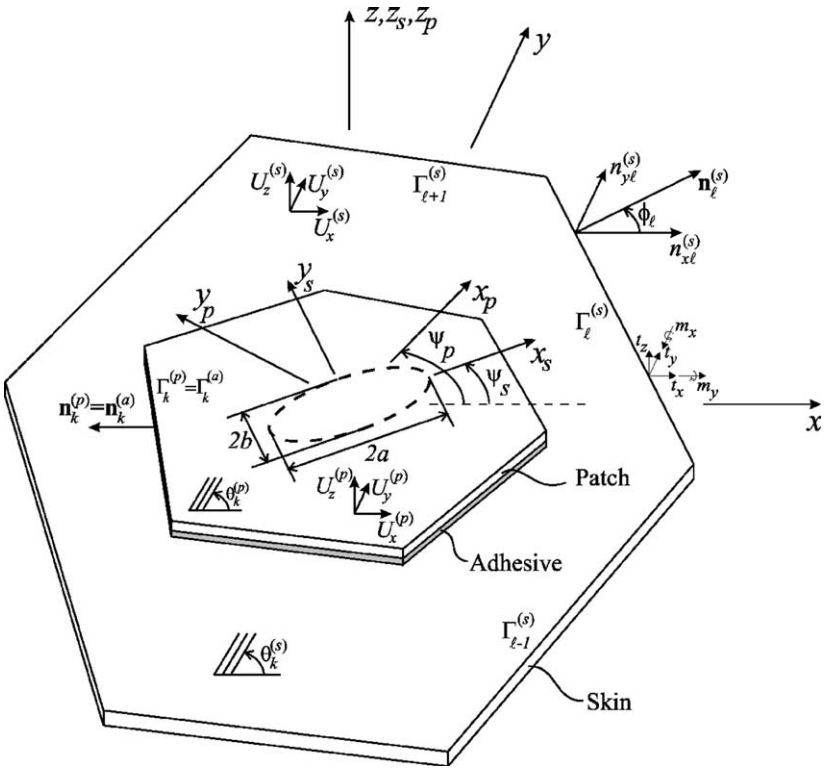

Fig. 1. Geometry and loading of a bonded patch–repaired skin with an elliptical cutout.

axis of length a and b, respectively. Two coordinate systems whose origins coincide with the center of the cutout are shown in Fig. 1. The global structural coordinates are given by (x, y, z), and the principal coordinates of the elliptical cutout are given by (x_s, y_s, z_s). The orientation of the cutout with respect to the global structural coordinates is defined by the angle ψ_s. Although not required, a local coordinate system, (x_p, y_p, z_p), with orientation angle ψ_p is also attached to the patch for consistency in the formulation.

As shown in Fig. 1, $\Gamma_\ell^{(s)}$ represents the ℓth boundary segment of the entire boundary. The unit normal to the ℓth boundary segment is represented by $\mathbf{n}_\ell^{(s)}$, with components $n_{x\ell}^{(s)}$ and $n_{y\ell}^{(s)}$ in the x-and y-directions, respectively. The unit normal, $\mathbf{n}_\ell^{(s)}$, makes an angle, ϕ_ℓ, with respect to the positive x-axis, as shown in Fig. 1. Similarly, the unit normals to the kth boundary, $\Gamma_k^{(\mathrm{p})} = \Gamma_k^{(\mathrm{a})}$, of the patch and adhesive are denoted by $\mathbf{n}_k^{(\mathrm{p})}$and $\mathbf{n}_k^{(\mathrm{a})}$, respectively.

The patch is attached to the skin by the adhesive and, therefore, its external boundaries are traction-free. The exterior edges of the skin are subjected to both in-plane tractions and bending moments. The in-plane external tractions include components t_x, t_y, and t_z, and the external bending tractions include components m_x and m_y. The traction components are defined with respect to the (x, y, z) structural coordinates, and their positive-valued directions are shown in Fig. 1. The global displacement components in the x-, y-, and z-directions are denoted by $U_x^{(d)}$, $U_y^{(d)}$, and $U_z^{(d)}$, with $d =$ s, p, a, respectively. The superscripts 'p', 's', and 'a' denote the patch, skin, and adhesive, respectively. Symmetrically laminated patch and skin are made of specially orthotropic layers, and each layer has an orientation angle, $\theta_k^{(d)}$, defined with respect to the positive x-axis (Fig. 1). Each layer has thickness $t_k^{(d)}$, elastic moduli $E_{\mathrm{L}}^{(d)}$ and $E_{\mathrm{T}}^{(d)}$, shear modulus $G_{\mathrm{LT}}^{(d)}$, and Poisson's ratio $v_{\mathrm{LT}}^{(d)}$, where L and T are the longitudinal (fiber) and transverse principal material directions, respectively.

The adhesive material is isotropic, homogeneous, and elastic, with a bi-linear relation between the effective transverse shear stress, $\tau_{\text{eff}}^{(a)}$, and effective transverse shear strain, $\gamma_{\text{eff}}^{(a)}$, as shown in Fig. 2. The effective transverse shear stress and strain are defined by

$$\tau_{\text{eff}}^{(a)} = \sqrt{\sigma_{xz}^{(a)^2} + \sigma_{yz}^{(a)^2}} \tag{1a}$$

and

$$\gamma_{\text{eff}}^{(a)} = \sqrt{\gamma_{xz}^{(a)^2} + \gamma_{yz}^{(a)^2}} \tag{1b}$$

in which $\sigma_{xz}^{(a)}, \sigma_{yz}^{(a)}$ and $\gamma_{xz}^{(a)}, \gamma_{yz}^{(a)}$ represent the components of the transverse shear stress and strain, respectively, in the adhesive. As shown in Fig. 2, the initial shear modulus of the bi-linear adhesive behavior is denoted by $G_1^{(a)}$ (it reduces to $G_2^{(a)}$ after the characteristic transverse shear strain, $\gamma_c^{(a)}$) and has a Poisson's ratio of $\nu^{(a)}$. With these parameters, the bi-linear relationship between the effective transverse shear stress, $\tau_{\text{eff}}^{(a)}$, and effective transverse shear strain, $\gamma_{\text{eff}}^{(a)}$, can be expressed as

$$\tau_{\text{eff}}^{(a)} = G_1^{(a)}\gamma_{\text{eff}}^{(a)}\left[1 - H\left(\gamma_{\text{eff}}^{(a)} - \gamma_c^{(a)}\right)\right] + \left[G_1^{(a)}\gamma_c^{(a)} + G_2^{(a)}\left(\gamma_{\text{eff}}^{(a)} - \gamma_c^{(a)}\right)\right]H\left(\gamma_{\text{eff}}^{(a)} - \gamma_c^{(a)}\right), \tag{2}$$

where $H(\gamma_{\text{eff}}^{(a)} - \gamma_c^{(a)})$ is the Heaviside step function.

In accordance with this relationship, the transverse shear stresses, $\sigma_{\alpha z}^{(a)}$, and strains, $\gamma_{\alpha z}^{(a)}$, are related by

$$\sigma_{\alpha z}^{(a)} = G_{\text{eff}}^{(a)}\gamma_{\alpha z}^{(a)} \quad \text{with } \alpha = x, y \tag{3}$$

in which the parameter $G_{\text{eff}}^{(a)}$ represents the effective shear modulus of the adhesive defined as

$$G_{\text{eff}}^{(a)} = \frac{\tau_{\text{eff}}^{(a)}}{\gamma_{\text{eff}}^{(a)}}. \tag{4}$$

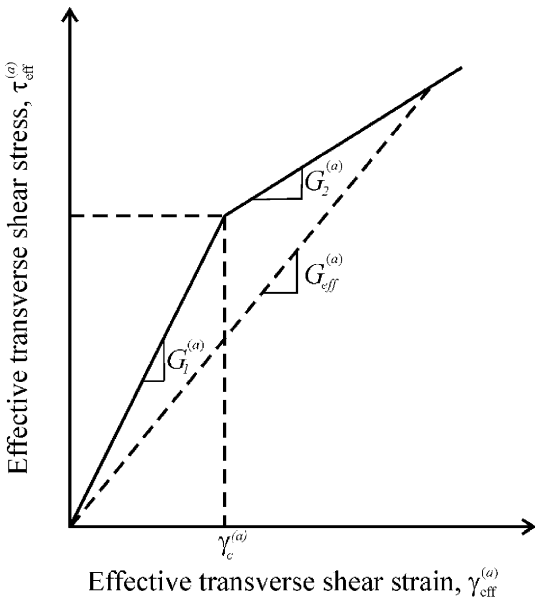

Fig. 2. Bi-linear elastic material model for the adhesive.

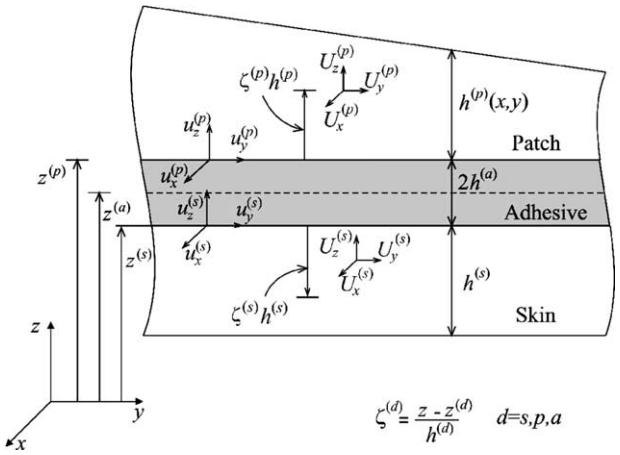

Fig. 3. Reference planes for kinematic relations of the patch, skin, and adhesive.

Furthermore, the transverse normal stress, $\sigma_{zz}^{(a)}$, and strain, $\varepsilon_{zz}^{(a)}$, in the adhesive are related by

$$\sigma_{zz}^{(a)} = E_{\text{eff}}^{(a)} \varepsilon_{zz}^{(a)} \tag{5}$$

in which $E_{\text{eff}}^{(a)}$ is the effective Young's modulus expressed as

$$E_{\text{eff}}^{(a)} = 2G_{\text{eff}}^{(a)}(1 + v^{(a)}). \tag{6}$$

The thicknesses of the skin and adhesive are uniform and denoted by $h^{(s)}$ and $2h^{(a)}$, respectively. As shown in Fig. 3, the patch can be tapered near the edges with a variable thickness $h^{(p)}(x, y)$. Also shown in Fig. 3 are the reference planes of the skin and patch, denoted by $z^{(d)}$ ($d = s, p$), and the fact that they do not coincide with their mid-surfaces. The reason for the choice of an eccentric reference location is apparent for the tapered patch because a flat plane exists only at its bottom surface. Although the mid-surface of the skin could serve as a reference plane, the choice of its top surface as the reference plane leads to simplified expressions for the transverse shear strain components in the adhesive. Due to the choice of these eccentric locations for reference planes for the adherents, the material property matrix includes the material coupling effects. As for the adhesive, its mid-surface, denoted by $z^{(a)}$, serves as the reference plane in describing the shear-lag model.

The problem posed here concerns the development of an analytical method to determine the displacement and stress fields in the repair of a skin with a hole by bonding a tapered patch over it while including the effect of geometric nonlinearity and bi-linear elastic adhesive material behaviors.

3. Solution method

The present nonlinear analysis method is based on the principle of virtual work in conjunction with a Rayleigh–Ritz approach. The displacement components are approximated in terms of the superposition of local and global functions, $\bar{u}_\alpha^{(d)}$ and $\bar{\bar{u}}_\alpha^{(d)}$, respectively, as

$$u_\alpha^{(d)} = \bar{u}_\alpha^{(d)} + \bar{\bar{u}}_\alpha^{(d)} \tag{7}$$

with $d = \mathrm{p}, \mathrm{s}$ and $\alpha = x, y, z$. The local displacement functions, $\bar{u}_{\alpha}^{(d)}$, are expressed as Laurent series in terms of complex functions in the form

$$\bar{u}_{x}^{(d)} = 2\mathrm{Re}\left[\sum_{k=1}^{2} d_{xk}^{(d)} \sum_{n=-N_{d1}}^{N_{d2}} \alpha_{nk}^{(d)} \Phi_{nk}^{(d)}\left(z_{\varepsilon k}^{(d)}\right)\right], \tag{8a}$$

$$\bar{u}_{y}^{(d)} = 2\mathrm{Re}\left[\sum_{k=1}^{2} d_{yk}^{(d)} \sum_{n=-N_{d1}}^{N_{d2}} \alpha_{nk}^{(d)} \Phi_{nk}^{(d)}\left(z_{\varepsilon k}^{(d)}\right)\right], \tag{8b}$$

$$\bar{u}_{z}^{(d)} = 2\mathrm{Re}\left[\sum_{k=1}^{2} \sum_{n=-N_{d1}}^{N_{d2}} \beta_{nk}^{(d)} F_{nk}^{(d)}\left(z_{\kappa k}^{(d)}\right)\right] \tag{8c}$$

with

$$d_{xk}^{(d)} = \cos\psi^{(d)} p_{k}^{(d)} - \sin\psi^{(d)} q_{k}^{(d)}, \tag{9a}$$

$$d_{yk}^{(d)} = \sin\psi^{(d)} p_{k}^{(d)} + \cos\psi^{(d)} q_{k}^{(d)} \tag{9b}$$

in which the explicit definitions of complex functions $\Phi_{nk}^{(d)}(z_{\varepsilon k}^{(d)})$ and $F_{nk}^{(d)}(z_{\kappa k}^{(d)})$ and the complex constants $p_{k}^{(d)}$ and $q_{k}^{(d)}$ are explicitly given in the Appendix A. The parameters N_{d1} and N_{d2}, with $d = \mathrm{p}, \mathrm{s}$, define the extent of the complex series, and the parameter N_{p1} is set to 0 because there is no cutout in the patch. In these series, $\alpha_{nk}^{(d)}$ and $\beta_{nk}^{(d)}$ are the unknown complex coefficients. These local functions satisfy the in-plane and bending equilibrium equations of a laminate exactly, as described by Madenci et al. (2001).

The global displacement functions, $\bar{\bar{u}}_{\alpha}^{(d)}$, are expressed as a series in terms of Chebyshev polynomials in reference to the global coordinates $(x, y$ in the form

$$\bar{\bar{u}}_{\alpha}^{(d)} = \sum_{m=0}^{M_d} \sum_{n=0}^{m} c_{\alpha(mn)}^{(d)} T_m(x) T_n(y) \tag{10}$$

in which $c_{\alpha(mn)}^{(d)}$, with $d = \mathrm{p}, \mathrm{s}$ and $\alpha = x, y, z$, are the unknown real coefficients. The parameter M_d specifies the extent of the series.

These local and global displacement functions can be expressed in matrix form as

$$\begin{aligned} \bar{u}_{x}^{(d)} &= \overline{\mathbf{V}}_{x}^{(d)^{\mathrm{T}}} \boldsymbol{\alpha}^{(d)} & & \bar{\bar{u}}_{x}^{(d)} = \overline{\bar{\mathbf{V}}}_{x}^{(d)^{\mathrm{T}}} \mathbf{c}_{x}^{(q)} \\ \bar{u}_{y}^{(d)} &= \overline{\mathbf{V}}_{y}^{(d)^{\mathrm{T}}} \boldsymbol{\alpha}^{(d)} \quad \text{and} & & \bar{\bar{u}}_{y}^{(d)} = \overline{\bar{\mathbf{V}}}_{y}^{(d)^{\mathrm{T}}} \mathbf{c}_{y}^{(q)} \\ \bar{u}_{z}^{(d)} &= \overline{\mathbf{V}}_{z}^{(d)^{\mathrm{T}}} \boldsymbol{\beta}^{(d)} & & \bar{\bar{u}}_{z}^{(d)} = \overline{\bar{\mathbf{V}}}_{z}^{(d)^{\mathrm{T}}} \mathbf{c}_{z}^{(q)} \end{aligned} \tag{11a, b}$$

in which the vectors $\boldsymbol{\alpha}^{(d)}$ and $\boldsymbol{\beta}^{(d)}$ contain the real and imaginary parts of the unknown coefficients $\alpha_{nk}^{(d)}$ and $\beta_{nk}^{(d)}$, respectively. The vectors $\mathbf{c}_{\alpha}^{(d)}$, with $\alpha = x, y, z$, contain the real unknown coefficients $c_{\alpha mn}^{(d)}$. The known vectors $\overline{\mathbf{V}}_{\alpha}^{(d)}$ and $\overline{\bar{\mathbf{V}}}_{\alpha}^{(d)}$ and their corresponding unknown coefficient vectors $\boldsymbol{\alpha}^{(d)}$ and $\boldsymbol{\beta}^{(d)}$ are defined explicitly in the Appendix A.

In matrix form, the approximate displacement representations given in Eq. (7) are rewritten as

$$\begin{aligned} u_{x}^{(d)} &= \mathbf{V}_{x}^{(d)^{\mathrm{T}}} \mathbf{q}^{(d)}, \\ u_{y}^{(d)} &= \mathbf{V}_{y}^{(d)^{\mathrm{T}}} \mathbf{q}^{(d)}, \\ u_{z}^{(d)} &= \mathbf{V}_{z}^{(d)^{\mathrm{T}}} \mathbf{q}^{(d)} \end{aligned} \tag{12}$$

in which the known vectors $\mathbf{V}_{\alpha}^{(d)}$, with $\alpha = x, y, z$, are defined as

$$\mathbf{V}_{x}^{(d)^{\mathrm{T}}} = \left\{ \overline{\mathbf{V}}_{x}^{(d)}, \overline{\overline{\mathbf{V}}}_{x}^{(d)}, \mathbf{0}, \mathbf{0}, \mathbf{0} \right\}, \tag{13a}$$

$$\mathbf{V}_{y}^{(d)^{\mathrm{T}}} = \left\{ \overline{\mathbf{V}}_{y}^{(d)}, \mathbf{0}, \overline{\overline{\mathbf{V}}}_{y}^{(d)}, \mathbf{0}, \mathbf{0} \right\}, \tag{13b}$$

$$\mathbf{V}_{z}^{(d)^{rmT}} = \left\{ \mathbf{0}, \mathbf{0}, \mathbf{0}, \overline{\mathbf{V}}_{z}^{(d)}, \overline{\overline{\mathbf{V}}}_{z}^{(d)} \right\}. \tag{13c}$$

In Eq. (12), the unknown vector $\mathbf{q}^{(d)}$ is defined as

$$\mathbf{q}^{(d)^{\mathrm{T}}} = \left\{ \boldsymbol{\alpha}^{(d)^{\mathrm{T}}}, \mathbf{c}_{x}^{(d)^{\mathrm{T}}}, \mathbf{c}_{y}^{(d)^{\mathrm{T}}}, \boldsymbol{\beta}^{(d)^{\mathrm{T}}}, \mathbf{c}_{z}^{(d)^{\mathrm{T}}} \right\}. \tag{14}$$

Note that the series representation of the displacement components is not required to satisfy any type of kinematic admissibility.

3.1. Kinematic relations

The patch and skin interact through the adhesive, which sustains transverse and shear deformations but not in-plane deformation. Both the patch and skin are subjected to in-plane and transverse deformations but not shear deformation. Also, the transverse normal and shear strain components are disregarded in the patch and skin because they are thin. Therefore, the in-plane strain components in the adhesive and the transverse normal and shear strain components in the patch and skin are not included in the derivation of the kinematic relations.

In accordance with the Kirchhoff plate theory, the global displacement components, $U_{x}^{(d)}$, $U_{y}^{(d)}$, and $U_{z}^{(d)}$, in the patch and the skin are defined as

$$U_{\alpha}^{(d)}(x,y,z) = u_{\alpha}^{(d)}(x,y) - \zeta^{(d)} h^{(d)} u_{z,\alpha}^{(d)}, \tag{15a}$$

$$U_{z}^{(d)}(x,y,z) = u_{z}^{(d)}(x,y) \tag{15b}$$

for which $d = p,s$ and $\alpha = x,y$; the displacement components, $u_{x}^{(d)}$, $u_{y}^{(d)}$, and $u_{z}^{(d)}$, are defined on the reference surfaces with respect to the global Cartesian coordinates (x,y,z), (Fig. 3). A subscript after a comma indicates differentiation with respect to the variable. As shown in Fig. 3, the coordinate $\zeta^{(d)}$ located on each of the reference planes is defined as

$$\zeta^{(d)} = \frac{z - z^{(d)}}{h^{(d)}} \quad \text{with } d = p,s \tag{16}$$

and varies in the range $-1 \zeta^{(\mathrm{s})} \leqslant 0$ in the skin and $0 \leqslant \zeta^{(\mathrm{p})} \leqslant 1$ in the patch. The thicknesses of the patch and skin are specified by $h^{(d)}$, and the location of the reference planes with respect to the global coordinate system (x,y,z) are defined by $z^{(d)}$, with $d = \mathrm{s}, \mathrm{p}$, as shown in Fig. 3.

3.2. Strain–displacement relations

The strain measures for the skin and patch are based on the modified form of Green's nonlinear strain–displacement relations in conjunction with von Karman assumptions for large deformation of plates (Fung and Tong, 2001). Therefore, the strain components in the skin and patch, $e_{\alpha\beta}^{(d)}$ ($d = \mathrm{p},\mathrm{s}$; $\alpha,\beta = x,y$), are expressed in terms of the displacement components as

$$e_{xx}^{(d)} = u_{x,x}^{(d)} - \zeta^{(d)} h^{(d)} u_{z,xx}^{(d)} + \frac{1}{2}\left(u_{z,x}^{(d)}\right)^2, \tag{17a}$$

$$e_{yy}^{(d)} = u_{y,y}^{(d)} - \zeta^{(d)} h^{(d)} u_{z,yy}^{(d)} + \frac{1}{2}\left(u_{z,y}^{(d)}\right)^2, \tag{17b}$$

$$e_{xy}^{(d)} = \frac{1}{2}\left(u_{x,y}^{(d)} + u_{y,x}^{(d)} - 2\zeta^{(d)} h^{(d)} u_{z,xy}^{(d)}\right) + \frac{1}{2} u_{z,x}^{(d)} u_{z,y}^{(d)}. \tag{17c}$$

In accordance with the von Karman nonlinear plate theory, the out-of plane displacements are on the order of the thickness, $h^{(d)}$, of the skin and patch and the derivatives of the in-plane displacement components are much smaller than those of the out-of-plane displacement components. These expressions for the strain components can be rewritten as

$$e_{xx}^{(d)} = \varepsilon_{xx}^{(d)} - \zeta^{(d)} h^{(d)} \kappa_{xx}^{(d)} + \frac{1}{2}(u_{z,x}^{(d)})^2, \tag{18a}$$

$$e_{yy}^{(d)} = \varepsilon_{yy}^{(d)} - \zeta^{(d)} h^{(d)} \kappa_{yy}^{(d)} + \frac{1}{2}\left(u_{z,y}^{(d)}\right)^2, \tag{18b}$$

$$e_{xy}^{(d)} = \frac{1}{2}\gamma_{xy}^{(d)} + \frac{1}{2}\zeta^{(d)} h^{(d)} \kappa_{xy}^{(d)} + \frac{1}{2} u_{z,x}^{(d)} u_{z,y}^{(d)} \tag{18c}$$

in which

$$\varepsilon_{xx}^{(d)} = u_{x,x}^{(d)}, \quad \kappa_{xx}^{(d)} = -u_{z,xx}^{(d)}, \tag{19a,b}$$

$$\varepsilon_{yy}^{(d)} = u_{y,y}^{(d)}, \quad \kappa_{yy}^{(q)} = -u_{z,yy}^{(q)}, \tag{19c,d}$$

$$\gamma_{xy}^{(d)} = u_{x,y}^{(d)} + u_{y,x}^{(d)}, \quad \kappa_{xy}^{(d)} = -2u_{z,xy}^{(d)}, \tag{19e,f}$$

where $\varepsilon_{xx}^{(d)}$, $\varepsilon_{yy}^{(d)}$, and $\gamma_{xy}^{(d)}$ represent the in-plane strain resultants and $\kappa_{xx}^{(d)}$, $\kappa_{yy}^{(d)}$, and $\kappa_{xy}^{(d)}$ represent the bending strain (curvature) resultants on the reference surfaces. Also, the in-plane and bending (curvature) strain resultants constitute the components of the linear part of the in-plane strain, $\boldsymbol{\varepsilon}_{\mathrm{L}}^{(d)}$, and curvature, $\boldsymbol{\kappa}_{\mathrm{L}}^{(d)}$, vectors in the form

$$\boldsymbol{\varepsilon}_{\mathrm{L}}^{(d)^{\mathrm{T}}} = \left\{\varepsilon_{xx}^{(d)}, \varepsilon_{yy}^{(d)}, \gamma_{xy}^{(d)}\right\} = \left\{u_{x,x}^{(d)}, u_{y,y}^{(d)}, u_{x,y}^{(d)} + u_{y,x}^{(d)}\right\}, \tag{20a}$$

$$\boldsymbol{\kappa}_{\mathrm{L}}^{(d)^{\mathrm{T}}} = \left\{\kappa_{xx}^{(d)}, \kappa_{yy}^{(d)}, \kappa_{xy}^{(d)}\right\} = \left\{-u_{z,xx}^{(d)}, -u_{z,yy}^{(d)}, -2u_{z,xy}^{(d)}\right\}. \tag{20b}$$

Similarly, the nonlinear terms appearing in the strain components, $e_{\alpha\beta}^{(d)}$ $(\alpha, \beta = x, y)$, are included in the nonlinear part of the in-plane strain resultant vector, $\varepsilon_{\mathrm{N}}^{(d)}$, in the form

$$\boldsymbol{\varepsilon}_{\mathrm{N}}^{(d)^{\mathrm{T}}} = \left\{\frac{1}{2}(u_{z,x}^{(d)})^2, \frac{1}{2}(u_{z,y}^{(d)})^2, u_{z,x}^{(d)} u_{z,y}^{(d)}\right\}. \tag{21}$$

Although the bending deformations (curvatures) are only linearly related to the out-of-plane displacement component, $u_z^{(d)}$, for consistency, a zero-valued vector is employed to represent the nonlinear part of the curvature vector, $\boldsymbol{\kappa}_{\mathrm{N}}^{(d)}$, as

$$\boldsymbol{\kappa}_{\mathrm{N}}^{(d)} = \{0, 0, 0\}. \tag{22}$$

Substituting for the derivatives of the displacement components from Eq. (12), the linear and nonlinear parts of the in-plane strain resultant and curvature vectors can be expressed as

$$\boldsymbol{\varepsilon}_{\mathrm{L}}^{(d)} = \mathbf{L}_{\varepsilon_{\mathrm{L}}}^{(d)}\mathbf{q}^{(d)}, \quad \boldsymbol{\kappa}_{\mathrm{L}}^{(d)} = \mathbf{L}_{\kappa_{\mathrm{L}}}^{(d)}\mathbf{q}^{(d)}, \tag{23a,b}$$

$$\boldsymbol{\varepsilon}_{\mathrm{N}}^{(d)} = \mathbf{L}_{\varepsilon_{\mathrm{N}}}^{(d)}(\mathbf{q}^{(d)})\mathbf{q}^{(d)}, \quad \boldsymbol{\kappa}_{\mathrm{N}}^{(d)} = 0, \tag{23c,d}$$

where

$$\mathbf{L}_{\varepsilon_{\mathrm{L}}}^{(d)} = \begin{bmatrix} \mathbf{V}_{x,x}^{(d)^{\mathrm{T}}} \\ \mathbf{V}_{y,y}^{(d)^{\mathrm{T}}} \\ \mathbf{V}_{x,y}^{(d)^{\mathrm{T}}} + \mathbf{V}_{y,x}^{(d)^{\mathrm{T}}} \end{bmatrix}, \tag{24a}$$

$$\mathbf{L}_{\kappa_{\mathrm{L}}}^{(d)} = -\begin{bmatrix} \mathbf{V}_{z,xx}^{(d)^{\mathrm{T}}} \\ \mathbf{V}_{z,yy}^{(d)^{\mathrm{T}}} \\ 2\mathbf{V}_{z,xy}^{(d)^{\mathrm{T}}} \end{bmatrix} \tag{24b}$$

and

$$\mathbf{L}_{\varepsilon_{\mathrm{N}}}^{(d)}(\mathbf{q}^{(d)}) = \frac{1}{2}\begin{bmatrix} u_{z,x}^{(d)}\mathbf{V}_{z,x}^{(d)^{\mathrm{T}}} \\ u_{z,y}^{(d)}\mathbf{V}_{z,y}^{(d)^{\mathrm{T}}} \\ u_{z,x}^{(d)}\mathbf{V}_{z,y}^{(d)^{\mathrm{T}}} + u_{z,y}^{(d)}\mathbf{V}_{z,x}^{(d)^{\mathrm{T}}} \end{bmatrix}. \tag{24c}$$

The vectors of strain resultants defined in Eq. (23) can be combined in a compact form as

$$\mathbf{e}_{\alpha}^{(d)} = \mathbf{L}_{\alpha}^{(d)}\mathbf{q}^{(d)} \quad \text{with } \alpha = \mathrm{L}, \mathrm{N}, \tag{25}$$

where

$$\mathbf{e}_{\alpha}^{(d)^{\mathrm{T}}} = \left\{\boldsymbol{\varepsilon}_{\alpha}^{(d)^{\mathrm{T}}}, \boldsymbol{\kappa}_{\alpha}^{(d)^{\mathrm{T}}}\right\}, \tag{26a}$$

$$\mathbf{L}_{\mathrm{L}}^{(d)} = \begin{bmatrix} \mathbf{L}_{\varepsilon_{\mathrm{L}}}^{(d)} \\ \mathbf{L}_{\kappa_{\mathrm{L}}}^{(d)} \end{bmatrix}, \tag{26b}$$

$$\mathbf{L}_{\mathrm{N}}^{(d)}(\mathbf{q}^{(d)}) = \begin{bmatrix} \mathbf{L}_{\varepsilon_{\mathrm{N}}}^{(d)}(\mathbf{q}^{(d)}) \\ \mathbf{0} \end{bmatrix}. \tag{26c}$$

Furthermore, the linear and nonlinear parts of the strain vectors, $\mathbf{e}_{\mathrm{L}}^{(d)}$ and $\mathbf{e}_{\mathrm{N}}^{(d)}$, can be added to form the total strain vector as

$$\mathbf{e}^{(d)} = \mathbf{e}_{\mathrm{L}}^{(d)} + \mathbf{e}_{\mathrm{N}}^{(d)} = \left[\mathbf{L}_{\mathrm{L}}^{(d)} + \mathbf{L}_{\mathrm{N}}^{(d)}(\mathbf{q}^{(d)})\right]\mathbf{q}^{(d)} = \mathbf{B}^{(d)}(\mathbf{q}^{(d)})\mathbf{q}^{(d)}, \tag{27}$$

where

$$\mathbf{B}^{(d)}(\mathbf{q}^{(d)}) = \mathbf{L}_{\mathrm{L}}^{(d)} + \mathbf{L}_{\mathrm{N}}^{(d)}(\mathbf{q}^{(d)}). \tag{28}$$

For the adhesive between the patch and the skin, the displacement components are assumed to vary linearly through the thickness. In order to ensure displacement continuity among the patch, adhesive, and skin, the displacement components for the adhesive are expressed as

$$U_{\alpha}^{(a)}(x,y,z) = \frac{1}{2}\left[U_{\alpha}^{(p)}(x,y,0) + U_{\alpha}^{(s)}(x,y,0)\right] + \frac{1}{2}^{(a)}\left[U_{\alpha}^{(p)}(x,y,0) - U_{\alpha}^{(s)}(x,y,0)\right] \tag{29}$$

with $\alpha = x, y, z$. Although the adhesive between the patch and skin undergoes the same magnitude of in-plane and transverse displacements as those of skin and the patch, the strain measure is based on a linear shear-lag model in which the transverse shear strain and the normal strain components in the adhesive are expressed in terms of the displacements in Eq. (29) as

$$\gamma_{\alpha z}^{(a)} = \frac{1}{2h^{(a)}}\left[U_{\alpha}^{(p)}(x,y,0) - U_{\alpha}^{(s)}(x,y,0)\right] + \frac{1}{2}\left[(1+\zeta^{(a)})U_{z,\alpha}^{(p)}(x,y,0) + (1-\zeta^{(a)})U_{z,\alpha}^{(s)}(x,y,0)\right], \tag{30a}$$

$$\varepsilon_{zz}^{(a)} = \frac{1}{2h^{(a)}}\left[U_{z}^{(p)}(x,y) - U_{z}^{(s)}(x,y)\right] \tag{30b}$$

with $\alpha = x,y$. The expressions for the transverse shear strain components, $\gamma_{\alpha z}^{(a)}(\alpha = x,y)$, are simplified to

$$\gamma_{\alpha z}^{(a)} = \frac{1}{2h^{(a)}}\left[U_{\alpha}^{(p)}(x,y,0) - U_{\alpha}^{(s)}(x,y,0)\right] \tag{31}$$

under the assumption that

$$U_{\alpha}^{(d)} \gg h^{(a)}U_{z,\beta}^{(d)} \quad (\alpha,\beta = x,y; d = s,p) \tag{32}$$

because the adhesive is an extremely thin layer.

Substituting for the displacement component evaluated at $\zeta^{(d)} = 0$ for $d = \mathrm{p,s}$ (the reference surface locations of the adherents) leads to

$$\gamma_{\alpha z}^{(a)} = \frac{1}{2h^{(a)}}\left[u_{\alpha}^{(p)}(x,y) - u_{\alpha}^{(s)}(x,y)\right] \quad \text{with } \alpha = x,y, \tag{33a}$$

$$\varepsilon_{zz}^{(a)} = \frac{1}{2h^{(a)}}\left[u_{z}^{(p)}(x,y) - u_{z}^{(s)}(x,y)\right]. \tag{33b}$$

Finally, substituting from Eq. (12) for the displacement components in Eq. (33) leads to the strain vector containing the transverse shear and normal strain components in the adhesive in matrix notation as

$$\boldsymbol{\varepsilon}^{(a)} = \mathbf{L}_{a}^{(p)}\mathbf{q}^{(p)} - \mathbf{L}_{a}^{(s)}\mathbf{q}^{(s)}, \tag{34}$$

where

$$\boldsymbol{\varepsilon}^{(a)^{\mathrm{T}}} = \left\{\gamma_{xz}^{(a)}, \gamma_{yz}^{(a)}, \varepsilon_{zz}^{(a)}\right\} \tag{35}$$

and the matrices $\mathbf{L}_{a}^{(p)}$ and $\mathbf{L}_{a}^{(s)}$ are defined as

$$\mathbf{L}_{a}^{(d)} = \frac{1}{2h^{(a)}}\begin{bmatrix}\mathbf{V}_{x}^{(d)^{\mathrm{T}}}\\ \mathbf{V}_{y}^{(d)^{\mathrm{T}}}\\ \mathbf{V}_{z}^{(d)^{\mathrm{T}}}\end{bmatrix} \quad \text{with } d = \mathrm{p,s}. \tag{36}$$

3.3. Stress–strain relations

The external in-plane loads acting along the boundary of the skin result not only in in-plane stresses but also in bending moments in both the patch and skin due the eccentricity between the mid-surfaces of the skin and patch and their interaction with the adhesive. The peeling stress in the adhesive is primarily due to the bending deformations arising from this load eccentricity.

The constitutive relations for both the skin and patch are based on the classical laminate theory, in which the stress resultants and moments are related to the strain resultants and curvatures in the form

$$\begin{Bmatrix} \mathbf{N}^{(s)} \\ \mathbf{M}^{(s)} \end{Bmatrix} = \begin{bmatrix} \mathbf{A}^{(s)} & \mathbf{B}^{(s)} \\ \mathbf{B}^{(s)} & \mathbf{D}^{(s)} \end{bmatrix} \begin{Bmatrix} \boldsymbol{\varepsilon}^{(s)} \\ \boldsymbol{\kappa}^{(s)} \end{Bmatrix}, \tag{37}$$

where

$$\begin{aligned} A_{ij}^{(s)} &= h^{(s)} \sum_{k=1}^{N_s} \left(\zeta_{k+1}^{(s)} - \zeta_k^{(s)}\right) \overline{Q}_{ij(k)}^{(s)}, \\ B_{ij}^{(s)} &= \frac{1}{2} h^{(s)^2} \sum_{k=1}^{N_s} \left(\zeta_{k+1}^{(s)^2} - \zeta_k^{(s)^2}\right) \overline{Q}_{ij(k)}^{(s)}, \\ D_{ij}^{(s)} &= \frac{1}{3} h^{(s)^3} \sum_{k=1}^{N_s} \left(\zeta_{k+1}^{(s)^3} - \zeta_k^{(s)^2}\right) \overline{Q}_{ij(k)}^{(s)} \end{aligned} \tag{38}$$

with

$$\zeta_k^{(s)} = \frac{z_k - z^{(s)}}{h^{(s)}} \quad (k = 1, \ldots, N_s \quad \text{and} \quad z^{(s)} - h^{(s)} \leqslant z_k \leqslant z^{(s)}) \tag{39}$$

and

$$\begin{Bmatrix} \mathbf{N}^{(p)} \\ \mathbf{M}^{(p)} \end{Bmatrix} = \begin{bmatrix} \mathbf{A}^{(p)}(x,y) & \mathbf{B}^{(p)}(x,y) \\ \mathbf{B}^{(p)}(x,y) & \mathbf{D}^{(p)}(x,y) \end{bmatrix} \begin{Bmatrix} \boldsymbol{\varepsilon}^{(p)} \\ \boldsymbol{\kappa}^{(p)} \end{Bmatrix}, \tag{40}$$

where

$$\begin{aligned} A_{ij}^{(p)}(x,y) &= h^{(p)}(x,y) \sum_{k=1}^{N_s} \left(\zeta_{k+1}^{(p)} - \zeta_k^{(p)}\right) \overline{Q}_{ij(k)}^{(p)}, \\ B_{ij}^{(p)}(x,y) &= \frac{1}{2} \left(h^{(p)}(x,y)\right)^2 \sum_{k=1}^{N_s} \left(\zeta_{k+1}^{(p)^2} - \zeta_k^{(p)^2}\right) \overline{Q}_{ij(k)}^{(p)}, \\ D_{ij}^{(p)}(x,y) &= \frac{1}{3} \left(h^{(p)}(x,y)\right)^3 \sum_{k=1}^{N_s} \left(\zeta_{k+1}^{(p)^3} - \zeta_k^{(p)^2}\right) \overline{Q}_{ij(k)}^{(p)} \end{aligned} \tag{41}$$

with

$$\zeta_k^{(p)} = \frac{z_k(x,y) - z^{(p)}}{h^{(p)}(x,y)} \quad (k = 1, \ldots, N_s \quad \text{and} \quad z^{(p)} z_k z^{(p)} + h^{(p)}). \tag{42}$$

In Eqs. (37) and (40), the matrices $\mathbf{A}^{(d)}$, $\mathbf{D}^{(d)}$, and $\mathbf{B}^{(d)}$ ($d = \mathrm{s}, \mathrm{p}$) are associated with in-plane, bending, and coupled in-plane and bending behaviors of the adherents, and $\overline{Q}_{ij(k)}^{(d)}$ ($d = \mathrm{s}, \mathrm{p}$) are the coefficients of the reduced stiffness matrix of the kth ply defined in the global x–y coordinate system. Note that the tapered patch thickness, $h^{(p)}$, varies as a function of the (x–y) coordinates. Hence, the material property matrices associated with the patch, $\mathbf{A}^{(p)}$, $\mathbf{B}^{(p)}$, and $\mathbf{D}^{(p)}$, are dependent on the plane coordinates (x–y) while those associated with the skin remain uniform.

Furthermore, the ratio of the ply thickness to the patch thickness is assumed to be constant, i.e., $t_k^{(p)}(x,y)/h^{(p)}(x,y) = \bar{t}_k^{(p)} = \text{constant}$. In this case, the material property matrices, $\mathbf{A}^{(p)}$, $\mathbf{B}^{(p)}$, and $D^{(p)}$, become dependent only on the patch thickness, $h^{(p)}$ (x, y).

The relations given in Eqs. (37) and (40) can be compacted in the form

$$\mathbf{s}^{(d)} = \mathbf{E}^{(d)}\mathbf{e}^{(d)} \quad \text{with } d = \mathrm{p}, \mathrm{s} \tag{43}$$

in which $\mathbf{s}^{(d)}$, $\mathbf{E}^{(d)}$, and $\mathbf{e}^{(d)}$ are defined as

$$\mathbf{s}^{(d)^{\mathrm{T}}} = \left\{\mathbf{N}^{(d)^{\mathrm{T}}}, \mathbf{M}^{(d)^{\mathrm{T}}}\right\}, \tag{44a}$$

$$\mathbf{E}^{(d)} = \begin{bmatrix} \mathbf{A}^{(d)} & \mathbf{B}^{(d)} \\ \mathbf{B}^{(d)} & \mathbf{D}^{(d)} \end{bmatrix}, \tag{44b}$$

$$\mathbf{e}^{(d)^{\mathrm{T}}} = \left\{\boldsymbol{\varepsilon}^{(d)^{\mathrm{T}}}, \boldsymbol{\kappa}^{(d)^{\mathrm{T}}}\right\}. \tag{44c}$$

With the representation of $\mathbf{e}^{(d)}$ in Eq. (27), the stress–strain relations given in Eq. (43) are re-expressed as

$$\mathbf{s}^{(d)} = \mathbf{E}^{(d)}\mathbf{B}^{(d)}(\mathbf{q}^{(d)})\mathbf{q}^{(d)}. \tag{45}$$

Because the adhesive does not sustain any in-plane deformation, the in-plane stress components, $\sigma_{xx}^{(\mathrm{a})}$, $\sigma_{yy}^{(\mathrm{a})}$, and $\sigma_{xy}^{(\mathrm{a})}$, are disregarded. The transverse shear stresses, $\sigma_{xz}^{(\mathrm{a})}$ and $\sigma_{yz}^{(\mathrm{a})}$, and the transverse normal stress, $\sigma_{zz}^{(\mathrm{a})}$, are related to the corresponding strain components through a bilinear relation as

$$\mathbf{s}^{(\mathrm{a})} = \mathbf{E}^{(\mathrm{a})}\boldsymbol{\varepsilon}^{(\mathrm{a})}, \tag{46}$$

where

$$\mathbf{s}^{(\mathrm{a})^{\mathrm{T}}} = h^{(\mathrm{a})}\left\{\sigma_{xz}^{(\mathrm{a})}, \sigma_{yz}^{(\mathrm{a})}, \sigma_{zz}^{(\mathrm{a})}\right\}, \tag{47a}$$

$$\boldsymbol{\varepsilon}^{(\mathrm{a})^{\mathrm{T}}} = \left\{\gamma_{xz}^{(\mathrm{a})}, \gamma_{yz}^{(\mathrm{a})}, \varepsilon_{zz}^{(\mathrm{a})}\right\}, \tag{47b}$$

$$\mathbf{E}^{(\mathrm{a})}(\mathbf{q}^{(\mathrm{s})}, \mathbf{q}^{(\mathrm{p})}) = \begin{bmatrix} G_{\mathrm{eff}}^{(\mathrm{a})}(\mathbf{q}^{(\mathrm{s})}, \mathbf{q}^{(\mathrm{p})}) & 0 & 0 \\ 0 & G_{\mathrm{eff}}^{(\mathrm{a})}(\mathbf{q}^{(\mathrm{s})}, \mathbf{q}^{(\mathrm{p})}) & 0 \\ 0 & 0 & E_{\mathrm{eff}}^{(\mathrm{a})}(\mathbf{q}^{(\mathrm{s})}, \mathbf{q}^{(\mathrm{p})}) \end{bmatrix} \tag{47c}$$

in which the expressions for $G_{\mathrm{eff}}^{(\mathrm{a})}(\mathbf{q}^{(\mathrm{s})}, \mathbf{q}^{(\mathrm{p})}) = G_{\mathrm{eff}}^{(\mathrm{a})}(\gamma_{\mathrm{eff}}^{(\mathrm{a})})$ and $E_{\mathrm{eff}}^{(\mathrm{a})}(\mathbf{q}^{(\mathrm{s})}, \mathbf{q}^{(\mathrm{p})}) = E_{\mathrm{eff}}^{(\mathrm{a})}(\gamma_{\mathrm{eff}}^{(\mathrm{a})})$ are defined in Eqs. (4) and (6), respectively.

Substituting for the expression for $\boldsymbol{\varepsilon}^{(\mathrm{a})}$ from Eq. (34) permits the stress–strain relations given in Eq. (46) to be expressed in terms of the unknowns of the skin and patch components as

$$\mathbf{s}^{(\mathrm{a})} = \mathbf{E}^{(\mathrm{a})}(\mathbf{q}^{(\mathrm{s})}, \mathbf{q}^{(\mathrm{p})})\left(\mathbf{L}_a^{(\mathrm{p})}\mathbf{q}^{(\mathrm{p})} - \mathbf{L}_a^{(\mathrm{s})}\mathbf{q}^{(\mathrm{s})}\right). \tag{48}$$

3.4. Boundary conditions

Along the ℓth segment of the skin boundary, $\Gamma_\ell^{(\mathrm{s})}$, as shown in Fig. 1, the prescribed displacement components normal and tangent to the boundary (${}^{(\ell)}\hat{u}_n^{(\mathrm{s})}$, ${}^{(\ell)}\hat{u}_t^{(\mathrm{s})}$, and ${}^{(\ell)}\hat{u}_z^{(\mathrm{s})}$) and the slope normal to the boundary (${}^{(\ell)}\hat{u}_{z,n}^{(\mathrm{s})}$) can be imposed as

$$\begin{aligned} u_n^{(\mathrm{s})} &= {}^{(\ell)}\hat{u}_n^{(\mathrm{s})}, \\ u_t^{(\mathrm{s})} &= {}^{(\ell)}\hat{u}_t^{(\mathrm{s})}, \\ u_z^{(\mathrm{s})} &= {}^{(\ell)}\hat{u}_z^{(\mathrm{s})}, \\ u_{z,n}^{(\mathrm{s})} &= {}^{(\ell)}\hat{u}_{z,n}^{(\mathrm{s})} \end{aligned} \tag{49}$$

Utilizing the vector representations of the displacement components given by Eq. (12), these prescribed displacements can be expressed as

$$\begin{aligned}
&\cos\phi_\ell \mathbf{V}_x^{(s)^T}\mathbf{q}^{(s)} + \sin\phi_\ell \mathbf{V}_y^{(s)^T}\mathbf{q}^{(s)} - {}^{(\ell)}\hat{u}_n^{(s)} = 0,\\
&-\sin\phi_\ell \mathbf{V}_x^{(s)^T}\mathbf{q}^{(s)} + \cos\phi_\ell \mathbf{V}_y^{(s)^T}\mathbf{q}^{(s)} - {}^{(\ell)}\hat{u}_t^{(s)} = 0,\\
&\mathbf{V}_z^{(s)^T}\mathbf{q}^{(s)} - {}^{(\ell)}\hat{u}_z^{(s)} = 0,\\
&\cos\phi_\ell \mathbf{V}_{z,x}^{(s)^T}\mathbf{q}^{(s)} + \sin\phi_\ell \mathbf{V}_{z,y}^{(s)^T}\mathbf{q}^{(s)} - {}^{(\ell)}\hat{u}_{z,n}^{(s)} = 0.
\end{aligned} \tag{50}$$

These equations are rewritten in compact form as

$$\mathbf{V}_\ell^{(s)^T}\mathbf{q}^{(s)} - \hat{\mathbf{u}}_n^{(s)} = \mathbf{0}, \tag{51}$$

where the matrix $\mathbf{V}_\ell^{(s)}$ and the vector $\hat{\mathbf{u}}_n^{(s)}$ are defined as

$$\mathbf{V}_\ell^{(s)^T} = \begin{bmatrix} \cos\phi_\ell \mathbf{V}_x^{(s)^T} + \sin\phi_\ell \mathbf{V}_y^{(s)^T} & \mathbf{0} \\ -\sin\phi_\ell \mathbf{V}_x^{(s)^T} + \cos\phi_\ell \mathbf{V}_y^{(s)^T} & \mathbf{0} \\ \mathbf{0} & \mathbf{V}_z^{(s)^T} \\ \mathbf{0} & \cos\phi_\ell \mathbf{V}_{z,x}^{(s)^T} + \sin\phi_\ell \mathbf{V}_{z,y}^{(s)^T} \end{bmatrix} \tag{52}$$

and

$$\hat{\mathbf{u}}_\ell^{(s)^T} = \left\{ {}^{(\ell)}\hat{u}_n^{(s)} \quad {}^{(\ell)}\hat{u}_t^{(s)} \quad {}^{(\ell)}\hat{u}_z^{(s)} \quad {}^{(\ell)}\hat{u}_{z,n}^{(s)} \right\}. \tag{53}$$

The boundary conditions in Eq. (51) are enforced as constraint conditions by introducing Lagrange multiplier functions, $\mathbf{\Lambda}_{\alpha\ell}^{(s)}(t)$, with $\alpha = n, t, z$, and $\mathbf{\Lambda}_{z\ell}^{\prime(s)}(t)$, defined along the ℓth boundary segment. These boundary conditions are written in integral form as

$$\int_{\Gamma_\ell^{(s)}} \mathbf{\Lambda}_\ell^{(s)}(t)\left\{\mathbf{V}_\ell^{(s)^T}\mathbf{q}^{(s)} - \hat{\mathbf{u}}_\ell^{(s)}\right\} \mathrm{d}t = 0, \tag{54}$$

where the matrix $\mathbf{\Lambda}_\ell^{(s)}$ contains the Lagrange multiplier functions in the form

$$\mathbf{\Lambda}_\ell^{(s)}(t) = \begin{bmatrix} \mathbf{\Lambda}_{n\ell}^{(s)}(t) & & & \\ & \mathbf{\Lambda}_{t\ell}^{(s)}(t) & & \\ & & \mathbf{\Lambda}_{z\ell}^{(s)}(t) & \\ & & & \mathbf{\Lambda}_{z\ell}^{\prime(s)}(t) \end{bmatrix}. \tag{55}$$

The Lagrange multiplier functions $\mathbf{\Lambda}_{\alpha\ell}^{(s)}(t)$, with $\alpha = n, t, z$, and $\mathbf{\Lambda}_{z\ell}^{\prime(s)}(t)$ are defined in terms of Legendre polynomials as

$$\left(\mathbf{\Lambda}_{\alpha\ell}^{(s)}\Big(t(\xi)\Big), \mathbf{\Lambda}_{z\ell}^{\prime(s)}(t(\xi))\right) = \sum_{j=0}^{J}\left(\lambda_{j(\alpha\ell)}^{(s)}, \lambda_{j(z\ell)}^{\prime(s)}\right) P_j(\xi), \tag{56}$$

where P_j represents the jth-order Legendre polynomial and $\lambda_{j(\alpha\ell)}$, with $\alpha = n, t, z$, and $\lambda'_{j(z\ell)}$ are the unknown Lagrange multipliers associated with each Legendre polynomial, P_j, and boundary segment, $\Gamma_\ell^{(s)}$.

Substituting the expressions for the Lagrange multiplier functions from Eq. (56) into Eq. (54) and rearranging the terms, the constraint equations representing the prescribed displacements can be rewritten as

$$\boldsymbol{\lambda}_{\ell}^{(\mathrm{s})^{\mathrm{T}}}\left(\mathbf{C}_{\ell}^{(\mathrm{s})}\mathbf{q}^{(\mathrm{s})}-\mathbf{f}_{\ell c}^{(\mathrm{s})}\right)=0 \quad \text{with } \ell=1,\ldots,L, \tag{57}$$

where

$$\boldsymbol{\lambda}_{\ell}^{(\mathrm{s})^{\mathrm{T}}}=\left\{\lambda_{1\ell}^{(\mathrm{s})^{\mathrm{T}}},\quad \lambda_{2\ell}^{(\mathrm{s})^{\mathrm{T}}},\quad \ldots,\quad \lambda_{J\ell}^{(\mathrm{s})^{\mathrm{T}}}\right\} \tag{58}$$

with

$$\boldsymbol{\lambda}_{k\ell}^{(\mathrm{s})^{\mathrm{T}}}=\left\{\lambda_{k(n\ell)}^{(\mathrm{s})},\quad \lambda_{k(t\ell)}^{(\mathrm{s})},\quad \lambda_{k(z\ell)}^{(\mathrm{s})},\quad \lambda_{k(z\ell)}^{\prime(s)}\right\}, \tag{59a}$$

$$\mathbf{C}_{\ell}^{(\mathrm{s})^{\mathrm{T}}}=\left[\mathbf{C}_{1\ell}^{(\mathrm{s})^{\mathrm{T}}}\quad \mathbf{C}_{2\ell}^{(\mathrm{s})^{\mathrm{T}}}\quad \cdots\quad \mathbf{C}_{J\ell}^{(\mathrm{s})^{\mathrm{T}}}\right], \tag{59b}$$

$$\mathbf{C}_{j\ell}^{(\mathrm{s})}=\int_{\Gamma_{\ell}^{(\mathrm{s})}}P_j\mathbf{V}_{\ell}^{(\mathrm{s})^{\mathrm{T}}}\mathrm{d}\Gamma \tag{60}$$

and

$$\mathbf{f}_{\ell c}^{(\mathrm{s})^{\mathrm{T}}}=\left\{\mathbf{f}_{1(\ell c)}^{(\mathrm{s})^{\mathrm{T}}},\quad \mathbf{f}_{2(\ell c)}^{(\mathrm{s})^{\mathrm{T}}},\quad \ldots,\quad \mathbf{f}_{J(\ell c)}^{(\mathrm{s})^{\mathrm{T}}}\right\} \tag{61}$$

with

$$\mathbf{f}_{j(\ell c)}^{(\mathrm{s})^{\mathrm{T}}}=\int_{\Gamma_{\ell}^{(\mathrm{s})}}P_j\hat{\mathbf{u}}_{\ell}^{(\mathrm{s})^{\mathrm{T}}}\mathrm{d}\Gamma. \tag{62}$$

The constraint equations in Eq. (57) can be assembled to form a single matrix equation combining all of the constraint equations as

$$\lambda^{(\mathrm{s})^{\mathrm{T}}}\left(\mathbf{C}^{(\mathrm{s})}\mathbf{q}^{(\mathrm{s})}-\mathbf{f}_{\mathrm{c}}^{(\mathrm{s})}\right)=0 \tag{63}$$

where

$$\lambda^{(\mathrm{s})^{\mathrm{T}}}=\left\{\lambda_{1}^{(\mathrm{s})^{\mathrm{T}}},\quad \lambda_{2}^{(\mathrm{s})^{\mathrm{T}}},\quad \ldots,\quad \lambda_{\mathrm{L}}^{(\mathrm{s})^{\mathrm{T}}}\right\}, \tag{64a}$$

$$\mathbf{C}^{(\mathrm{s})^{\mathrm{T}}}=\left[\mathbf{C}_{1}^{(\mathrm{s})^{\mathrm{T}}}\quad \mathbf{C}_{2}^{(\mathrm{s})^{\mathrm{T}}}\quad \cdots\quad \mathbf{C}_{\mathrm{L}}^{(\mathrm{s})^{\mathrm{T}}}\right], \tag{64b}$$

$$\mathbf{f}_{\mathrm{c}}^{(\mathrm{s})^{\mathrm{T}}}=\left\{\mathbf{f}_{1c}^{(\mathrm{s})^{\mathrm{T}}},\quad \mathbf{f}_{2c}^{(\mathrm{s})^{\mathrm{T}}},\quad \ldots,\quad \mathbf{f}_{Lc}^{(\mathrm{s})^{\mathrm{T}}}\right\}. \tag{64c}$$

The system of constraint equations in Eq. (63) is unique, provided the rank of the matrix $\mathbf{C}^{(\mathrm{s})}$ is equal to the total number of constraint equations. Also, Eq. (63) can be treated as the potential energy of the reaction forces producing zero energy since $(\mathbf{C}^{(\mathrm{s})}\mathbf{q}^{(\mathrm{s})}-\mathbf{f}_{\mathrm{c}}^{(\mathrm{s})})=\mathbf{0}$, and it can be referred to as the potential energy of the constraint forces, V_c, in the form

$$V_{\mathrm{c}}=\lambda^{(\mathrm{s})^{\mathrm{T}}}\left(\mathbf{C}^{(\mathrm{s})}\mathbf{q}^{(\mathrm{s})}-\mathbf{f}_{\mathrm{c}}^{(\mathrm{s})}\right)=0. \tag{65}$$

3.5. Governing equations

The governing equations are derived based on the principle of virtual work as explained by Washizu (1982)

$$\delta W_{\mathrm{i}}=\delta W_{\mathrm{e}}, \tag{66}$$

where δW_{i} and δW_{e} represent the virtual work due to internal and external forces, respectively, of the repaired skin.

The internal virtual work, δW_{i}, is the sum of the internal virtual work of the skin, patch, and the adhesive, i.e.,

$$\delta W_i = \delta W_i^{(\mathrm{s})} + \delta W_i^{(\mathrm{p})} + \delta W_i^{(\mathrm{a})}, \tag{67}$$

where the internal virtual work in the patch, skin, and adhesive is expressed as

$$\delta W_i^{(d)} = \int_{A_d} \delta \mathbf{e}^{(d)^{\mathrm{T}}} \mathbf{s}^{(d)} \mathrm{d}A = \int_{A_d} \delta \mathbf{e}^{(d)^{\mathrm{T}}} \mathbf{E}^{(d)} \mathbf{e}^{(d)} \mathrm{d}A \quad \text{with } d = \mathrm{p}, \mathrm{s} \tag{68}$$

and

$$\delta W_i^{(\mathrm{a})} = \int_{A_a} \delta \boldsymbol{\varepsilon}^{(\mathrm{a})^{\mathrm{T}}} \mathbf{s}^{(\mathrm{a})} \mathrm{d}A = \int_{A_a} \delta \boldsymbol{\varepsilon}^{(\mathrm{a})^{\mathrm{T}}} \mathbf{E}^{(\mathrm{a})} \boldsymbol{\varepsilon}^{(\mathrm{a})} \mathrm{d}A, \tag{69}$$

where A_d ($d = \mathrm{p}, \mathrm{s}, \mathrm{a}$) denotes the areas of the skin, patch, and adhesive.

Substituting from Eq. (27) and (34) and with the property of $\delta[\mathbf{L}_{\mathrm{N}}^{(d)}(\mathbf{q}^{(d)})]\mathbf{q}^{(d)} = \mathbf{L}_{\mathrm{N}}^{(d)}(\mathbf{q}^{(d)})\delta\mathbf{q}^{(d)}$, the total virtual strain vectors, $\delta\boldsymbol{\varepsilon}^{(\mathrm{a})}$ and $\delta\mathbf{e}^{(d)}$ are obtained as

$$\delta \boldsymbol{\varepsilon}^{(\mathrm{a})} = \delta \mathbf{q}^{(\mathrm{p})^{\mathrm{T}}} \mathbf{L}_a^{(\mathrm{p})} - \delta \mathbf{q}^{(\mathrm{s})} \mathbf{L}_a^{(\mathrm{s})^{\mathrm{T}}} \tag{70}$$

and

$$\delta \mathbf{e}^{(d)} = [\mathbf{L}_{\mathrm{L}}^{(d)} + 2\mathbf{L}_{\mathrm{N}}^{(d)}(\mathbf{q}^{(d)})]\delta\mathbf{q}^{(d)} = {}^{*}\mathbf{B}^{(d)}(\mathbf{q}^{(d)})\delta\mathbf{q}^{(d)}, \tag{71a}$$

where

$${}^{*}\mathbf{B}^{(d)}(\mathbf{q}^{(d)}) = \mathbf{L}_{\mathrm{L}}^{(d)} + 2\mathbf{L}_{\mathrm{N}}^{(d)}(\mathbf{q}^{(d)}). \tag{71b}$$

The external virtual work is expressed as the sum of the virtual work due to externally applied forces, $\delta W_{\mathrm{e}}^{(\mathrm{s})}$, and that arising from the boundary reaction forces, $\delta W_{\mathrm{c}}^{(\mathrm{s})}$, i.e.,

$$\delta W_{\mathrm{e}} = \delta W_{\mathrm{e}}^{(\mathrm{s})} + \delta W_{\mathrm{c}}^{(\mathrm{s})}. \tag{72}$$

The virtual work due to externally applied forces, $\delta W_{\mathrm{e}}^{(\mathrm{s})}$, is obtained from

$$\delta W_{\mathrm{e}}^{(\mathrm{s})} = \int_{\Gamma^{(\mathrm{s})}} \{\delta u_x^{(\mathrm{s})} t_x + \delta u_y^{(\mathrm{s})} t_y + \delta u_z^{(\mathrm{s})} t_z + \delta u_{z,x}^{(\mathrm{s})} m_x + \delta u_{z,y}^{(\mathrm{s})} m_y\} \mathrm{d}\Gamma, \tag{73}$$

where the external boundary of the skin is denoted by $\Gamma^{(\mathrm{s})}$, the applied tractions by t_x, t_y, and t_z, and the moments by m_x and m_y; their positive signs are shown in Fig. 1. Substituting for the displacement components and their derivatives from Eq. (12) permits this expression in matrix notation as

$$\delta W_{\mathrm{e}}^{(\mathrm{s})} = \delta \mathbf{q}^{(\mathrm{s})^{\mathrm{T}}} \mathbf{p}^{(\mathrm{s})} \tag{74}$$

in which

$$\mathbf{p}^{(\mathrm{s})^{\mathrm{T}}} = \left\{ \mathbf{p}_{\varepsilon}^{(\mathrm{s})^{\mathrm{T}}}, \mathbf{p}_{\kappa}^{(\mathrm{s})^{\mathrm{T}}} \right\} \tag{75}$$

with

$$\mathbf{p}_{\varepsilon}^{(\mathrm{s})} = \int_{\Gamma^{(\mathrm{s})}} \left\{ \mathbf{V}_x^{(\mathrm{s})} t_x + \mathbf{V}_y^{(\mathrm{s})} t_y \right\} \mathrm{d}\Gamma, \tag{76a}$$

$$\mathbf{p}_{\kappa}^{(\mathrm{s})} = \int_{\Gamma^{(\mathrm{s})}} \left\{ \mathbf{V}_z^{(\mathrm{s})} t_z + \mathbf{V}_{z,x}^{(\mathrm{s})} m_x + \mathbf{V}_{z,y}^{(\mathrm{s})} m_y \right\} \mathrm{d}\Gamma. \tag{76b}$$

The virtual work due to the boundary reaction forces, $\delta W_c^{(s)}$, is identical to the first variation of the potential energy expression in Eq. (65) as

$$\delta W_c^{(s)} = -\delta V_c = -\delta\lambda^{(s)^T}(\mathbf{C}^{(s)}\mathbf{q}^{(s)} - \mathbf{f}_c^{(s)}) - \delta\mathbf{q}^{(s)^T}\mathbf{C}^{(s)^T}\lambda^{(s)}. \tag{77}$$

The virtual work due to boundary reactions (constraint conditions) can be interpreted as the virtual work of the constraint forces, $\lambda^{(s)}$, over the virtual displacements, $\delta(\mathbf{C}^{(s)}\mathbf{q}^{(s)})$, of the skin and the virtual work of the constrained displacements (boundary conditions), $\mathbf{C}^{(s)}\mathbf{q}^{(s)} - \mathbf{f}_c^{(s)}$, over the virtual constraint forces, $\delta\lambda^{(s)}$. Although the term $(\mathbf{C}^{(s)}\mathbf{q}^{(s)} - \mathbf{f}_c^{(s)})$ is identical to zero, it is included in the virtual work expression in order to obtain a complete set of equations that contain both equilibrium equations and constraint conditions.

Substituting from Eqs. (68), (69), (74) and (77), the principle of virtual work from Eq. (66) is rewritten as

$$\begin{aligned}&\int_{A_s}\delta\mathbf{e}^{(s)^T}\mathbf{E}^{(s)}\mathbf{e}^{(s)}\mathrm{d}A + \int_{A_p}\delta\mathbf{e}^{(p)^T}\mathbf{E}^{(p)}\mathbf{e}^{(p)}\mathrm{d}A + \int_{A_a}\delta\boldsymbol{\varepsilon}^{(a)^T}\mathbf{E}^{(a)}\boldsymbol{\varepsilon}^{(a)}\mathrm{d}A\\ &= \delta\mathbf{q}^{(s)^T}\mathbf{p}^{(s)} - \delta\lambda^{(s)^T}(\mathbf{C}^{(s)}\mathbf{q}^{(s)} - \mathbf{f}_c^{(s)}) - \delta\mathbf{q}^{(s)^T}\mathbf{C}^{(s)^T}\lambda^{(s)}.\end{aligned} \tag{78}$$

Substituting for the strain vectors, $\mathbf{e}^{(d)}$ ($d = \mathrm{s}, \mathrm{p}$) and $\boldsymbol{\varepsilon}^{(a)}$, from Eq. (27) and (34), and their virtual forms, $\delta\mathbf{e}^{(d)}$ ($d = \mathrm{s}, \mathrm{p}$) and $\delta\boldsymbol{\varepsilon}^{(a)}$, from Eq. (70) and (71), and rearranging the terms, the virtual work expression is recast into a compact form as

$$\begin{aligned}&\delta\mathbf{q}^{(s)^T}\left(\mathbf{K}^{(s)}(\mathbf{q}^{(s)}) + \mathbf{K}_{ss}^{(a)}(\mathbf{q}^{(p)},\mathbf{q}^{(s)})\right)\mathbf{q}^{(s)} + \delta\mathbf{q}^{(p)^T}\left(\mathbf{K}^{(p)}(\mathbf{q}^{(p)}) + \mathbf{K}_{pp}^{(a)}(\mathbf{q}^{(p)},\mathbf{q}^{(s)})\right)\mathbf{q}^{(p)}\\ &- \delta\mathbf{q}^{(p)^T}\mathbf{K}_{ps}^{(a)}(\mathbf{q}^{(p)},\mathbf{q}^{(s)})\mathbf{q}^{(s)} - \delta\mathbf{q}^{(s)^T}\mathbf{K}_{sp}^{(a)}(\mathbf{q}^{(p)},\mathbf{q}^{(s)})\mathbf{q}^{(p)}\\ &= \delta\mathbf{q}^{(s)^T}\mathbf{p}^{(s)} - \delta\boldsymbol{\lambda}^{(s)^T}\mathbf{C}^{(s)}\mathbf{q}^{(s)} - \delta\mathbf{q}^{(s)^T}\mathbf{C}^{(s)^T}\lambda^{(s)} + \delta\boldsymbol{\lambda}^{(s)^T}\mathbf{f}_c^{(s)},\end{aligned} \tag{79}$$

where

$$\mathbf{K}^{(d)}(\mathbf{q}^{(d)}) = \int_{A_d} {}^*\mathbf{B}^{(d)^T}(\mathbf{q}^{(d)})\mathbf{E}^{(d)}\mathbf{B}^{(d)}(\mathbf{q}^{(d)})\mathrm{d}A \quad (d = \mathrm{s}, \mathrm{p}), \tag{80a}$$

$$\mathbf{K}_{\alpha\beta}^{(a)}(\mathbf{q}^{(p)},\mathbf{q}^{(s)}) = \int_{A_a}\mathbf{L}_a^{(\alpha)^T}\mathbf{E}^{(a)}(\mathbf{q}^{(p)},\mathbf{q}^{(s)})\mathbf{L}_a^{(\beta)}\mathrm{d}A \quad (\alpha,\beta = \mathrm{s}, \mathrm{p}). \tag{80b}$$

The principle of virtual work from Eq. (79) can further be rearranged and put into a more compact form as

$$\begin{Bmatrix}\delta\mathbf{q}^{(s)^T}\\ \delta\mathbf{q}^{(p)^T}\\ \delta\lambda^{(s)^T}\end{Bmatrix}\begin{bmatrix}\mathbf{K}_{ss}(\mathbf{q}^{(p)},\mathbf{q}^{(s)}) & \mathbf{K}_{sp}(\mathbf{q}^{(p)},\mathbf{q}^{(s)}) & \mathbf{C}^{(s)^T}\\ \mathbf{K}_{sp}^T(\mathbf{q}^{(p)},\mathbf{q}^{(s)}) & \mathbf{K}_{pp}(\mathbf{q}^{(p)},\mathbf{q}^{(s)}) & \mathbf{0}\\ \mathbf{C}^{(s)} & \mathbf{0} & \mathbf{0}\end{bmatrix}\begin{Bmatrix}\mathbf{q}^{(s)}\\ \mathbf{q}^{(p)}\\ \boldsymbol{\lambda}^{(s)}\end{Bmatrix} - \begin{Bmatrix}\delta\mathbf{q}^{(s)^T}\\ \delta\mathbf{q}^{(p)^T}\\ \delta\boldsymbol{\lambda}^{(s)^T}\end{Bmatrix}\begin{Bmatrix}\mathbf{p}^{(s)}\\ \mathbf{0}\\ \mathbf{f}_c\end{Bmatrix} = 0, \tag{81}$$

where

$$\mathbf{K}_{ss}(\mathbf{q}^{(p)},\mathbf{q}^{(s)}) = \mathbf{K}^{(s)}(\mathbf{q}^{(s)}) + \mathbf{K}_{ss}^{(a)}(\mathbf{q}^{(p)},\mathbf{q}^{(s)}), \tag{82a}$$

$$\mathbf{K}_{pp}(\mathbf{q}^{(p)},\mathbf{q}^{(s)}) = \mathbf{K}^{(p)}(\mathbf{q}^{(p)}) + \mathbf{K}_{pp}^{(a)}(\mathbf{q}^{(p)},\mathbf{q}^{(s)}), \tag{82b}$$

$$\mathbf{K}_{sp}(\mathbf{q}^{(p)},\mathbf{q}^{(s)}) = -\mathbf{K}_{sp}^{(a)}(\mathbf{q}^{(p)},\mathbf{q}^{(s)}), \tag{82c}$$

$$\mathbf{K}_{ps}(\mathbf{q}^{(p)},\mathbf{q}^{(s)}) = -\mathbf{K}_{ps}^{(a)}(\mathbf{q}^{(p)},\mathbf{q}^{(s)}) = \mathbf{K}_{sp}^T(\mathbf{q}^{(p)},\mathbf{q}^{(s)}). \tag{82d}$$

For arbitrary variations of the virtual solution vectors $\delta\mathbf{q}^{(s)}$, $\delta\mathbf{q}^{(p)}$, and $\delta\boldsymbol{\lambda}^{(s)}$, the solution to Eq. (81) is obtained only if

$$\begin{bmatrix} \mathbf{K}_{ss}(\mathbf{q}^{(p)},\mathbf{q}^{(s)}) & \mathbf{K}_{sp}(\mathbf{q}^{(p)},\mathbf{q}^{(s)}) & \mathbf{C}^{(s)^T} \\ \mathbf{K}_{sp}^T(\mathbf{q}^{(p)},\mathbf{q}^{(s)}) & \mathbf{K}_{pp}(\mathbf{q}^{(p)},\mathbf{q}^{(s)}) & \mathbf{0} \\ \mathbf{C}^{(s)} & \mathbf{0} & \mathbf{0} \end{bmatrix} \begin{Bmatrix} \mathbf{q}^{(s)} \\ \mathbf{q}^{(p)} \\ \lambda^{(s)} \end{Bmatrix} = \begin{Bmatrix} \mathbf{p}^{(s)} \\ \mathbf{0} \\ \mathbf{f}_c \end{Bmatrix}. \tag{83}$$

Note that the resulting governing equations are nonlinear and the matrices $\mathbf{K}_{ss}(\mathbf{q}^{(p)}, \mathbf{q}^{(s)})$ and $\mathbf{K}_{pp}$ $(\mathbf{q}^{(p)}, \mathbf{q}^{(s)})$ are non-symmetric. The solution to this equation requires a nonlinear iterative solution technique that utilizes **LU** decomposition. Therefore, the Newton–Raphson iteration method, in conjunction with Broyden's automatic Jacobian matrix update procedure, is employed.

The nonlinear equilibrium equation, Eq. (83), can be rearranged in the form

$$\boldsymbol{\psi}(\mathbf{q}) = \mathbf{K}(\mathbf{q})\mathbf{q} - \mathbf{f} = \mathbf{0}, \tag{84}$$

where the vectors $\mathbf{q}$ and $\mathbf{f}$ and the matrix $\mathbf{K}(\mathbf{q})$ are defined as

$$\mathbf{q}^T = \left\{\mathbf{q}^{(s)^T}, \mathbf{q}^{(p)^T}, \boldsymbol{\lambda}^{(s)^T}\right\}, \tag{85a}$$

$$\mathbf{f}^T = \left\{\mathbf{p}^T, \mathbf{0}^T, \mathbf{f}_c^T\right\}, \tag{85b}$$

$$\mathbf{K}(\mathbf{q}) = \begin{bmatrix} \mathbf{K}_{ss}(\mathbf{q}) & \mathbf{K}_{sp}(\mathbf{q}) & \mathbf{C}^{(s)^T} \\ \mathbf{K}_{sp}^T(\mathbf{q}) & \mathbf{K}_{pp}(\mathbf{q}) & \mathbf{0} \\ \mathbf{C}^{(s)} & \mathbf{0} & \mathbf{0} \end{bmatrix}. \tag{85c}$$

The vector $\boldsymbol{\psi}(\mathbf{q})$ represents the unbalanced load vector. Under equilibrium conditions, the solution vector $\mathbf{q}$ exactly satisfies Eq. (84) and no unbalanced forces exist. However, it is practically impossible to obtain a direct solution of the nonlinear equilibrium equations. Instead, the solution is obtained by resorting to an iterative procedure, such as the Newton–Raphson (N–R) method. In order to proceed with the N–R method, Eq. (84) is rewritten in iterative form as

$$\boldsymbol{\psi}(\mathbf{q}_m^{k+1}) = \mathbf{K}(\mathbf{q}_m^{k+1})\mathbf{q}_m^{k+1} - \mathbf{f}_m = \mathbf{0}, \tag{86}$$

where $\mathbf{q}_m^{k+1}$ denotes the trial solution vector at load step m after k iterations, and it is expressed as a correction to the trial solution vector, $\mathbf{q}_m^k$, at the kth iteration at load step m, i.e.,

$$\mathbf{q}_m^{k+1} = \mathbf{q}_m^k + \Delta\mathbf{q} \tag{87}$$

in which $\Delta\mathbf{q}$ represents the correction term (incremental solution vector). The solution vector $\mathbf{q}_m^k$ is known from the kth iteration at load step $m$and the correction term, $\Delta\mathbf{q}$, is to be determined.

The Taylor series expansion of $\boldsymbol{\psi}(\mathbf{q}_m^{k+1})$ about the known trial solution $\mathbf{q}_m^k$ is

$$\boldsymbol{\psi}(\mathbf{q}_m^{k+1}) = \boldsymbol{\psi}(\mathbf{q}_m^k) + \frac{\partial\boldsymbol{\psi}}{\partial\mathbf{q}}(\mathbf{q}_m^k)\Delta\mathbf{q} + \mathrm{HOT} = 0 \tag{88}$$

in which the unbalanced load vector $\boldsymbol{\psi}(\mathbf{q}_m^k)$ is non-zero from the kth trial solution vector, $\mathbf{q}_m^k$. Retaining the linear terms in the expansion while disregarding the higher-order terms (HOT), the Newton–Raphson (N–R) method yields

$$\mathbf{J}(\mathbf{q}_m^k)\Delta\mathbf{q} = -\boldsymbol{\psi}(\mathbf{q}_m^k), \tag{89}$$

where the Jacobian matrix, $\mathbf{J}(\mathbf{q}_m^k)$, is defined as

$$\mathbf{J}(\mathbf{q}_m^k) = \frac{\partial \boldsymbol{\psi}}{\partial \mathbf{q}}(\mathbf{q}_m^k) = \frac{\partial \mathbf{K}}{\partial \mathbf{q}}(\mathbf{q}_m^k)\mathbf{q}_m^k + \mathbf{K}(\mathbf{q}_m^k) \tag{90}$$

and

$$\Delta\mathbf{q} = \mathbf{q}_m^{k+1} - \mathbf{q}_m^k. \tag{91}$$

Because of the linearization of Eq. (88), the incremental solution vector (the correction term), $\Delta\mathbf{q}$, obtained from Eq. (89) is not expected to yield the actual solution. However, it provides a good estimate of $\mathbf{q}_m^{k+1}$ in the form

$$\mathbf{q}_m^{k+1} = \mathbf{q}_m^k - \mathbf{J}^{-1}(\mathbf{q}_m^k)\boldsymbol{\psi}(\mathbf{q}_m^k). \tag{92}$$

As part of the iterative solution procedure, this recursive relationship requires the updated Jacobian matrix, i.e., $\mathbf{J}(\mathbf{q}_m^{k+1})$, which is obtained based on Broyden's algorithm (Geradin et al., 1981)

$$\mathbf{J}(\mathbf{q}_m^{k+1}) = \mathbf{J}(\mathbf{q}_m^k) + \frac{[\Delta\boldsymbol{\psi} - \mathbf{J}(\mathbf{q}_m^k)\Delta\mathbf{q}]\Delta\mathbf{q}^{\mathrm{T}}}{\Delta\mathbf{q}^{\mathrm{T}}\Delta\mathbf{q}}, \tag{93}$$

where

$$\Delta\boldsymbol{\psi} = \boldsymbol{\psi}(\mathbf{q}_m^{k+1}) - \boldsymbol{\psi}(\mathbf{q}_m^k). \tag{94}$$

At the beginning of the current (mth) load step, the converged solution vector, $\mathbf{q}_{m-1}^k$, and the Jacobian matrix, $\mathbf{J}(\mathbf{q}_{m-1}^k)$, computed from the previous load step are employed as the initial estimates for the solution vector and the Jacobian matrix in the current load step, i.e.,

$$\mathbf{q}_m^0 = \mathbf{q}_{m-1}^k = \mathbf{q}_{m-1} \quad \text{and} \quad \mathbf{J}(\mathbf{q}_m^0) = \mathbf{J}(\mathbf{q}_{m-1}^k) = \mathbf{J}(\mathbf{q}_{m-1}), \tag{95a, b}$$

where the superscripts on the right-hand sides of Eq. (95a, b) are removed to represent the converged solutions from the preceding load step.

Note that for the case of $k = m = 0$ (i.e., $\mathbf{q}_0^0 = \mathbf{0}$), the Jacobian matrix $\mathbf{J}(\mathbf{q}_0^0 = \mathbf{0})$ represents the linear stiffness matrix at the unloaded state of the patch-repaired skin, i.e.,

$$\mathbf{J}(\mathbf{q}_0^0 = \mathbf{0}) = \mathbf{K}(\mathbf{q}^{(\mathrm{p})} = 0, \mathbf{q}^{(\mathrm{s})} = 0) = \mathbf{K}_{\mathrm{L}}. \tag{96}$$

Therefore, the initial solution vector and the Jacobian matrix in the first load step are estimated by

$$\mathbf{q}_1^0 = \mathbf{0} \quad \text{and} \quad \mathbf{J}(\mathbf{q}_1^0) = \mathbf{K}_{\mathrm{L}}. \tag{97}$$

4. Numerical results

Before demonstrating the applicability of the present approach, its validity is established first by comparison against the experimental measurements for an untapered patch $\delta = 0$ presented by Barut et al. (2002). Then, its applicability is demonstrated by considering two patch–repair configurations. The first configuration is a tapered aluminum patch bonded over a circular cutout in an aluminum skin with a linear elastic adhesive material. The second configuration is an untapered composite patch bonded over a circular cutout in a composite skin with a bi-linear elastic adhesive material.

Arising from the presence of symmetry in geometry and loading for both the validation and demonstration cases, the displacement component, $\bar{\bar{u}}_x^{(q)}$, is symmetric in the x-direction while asymmetric in the

y-direction and $bar\bar{u}_y^{(q)}$ is asymmetric in the x-direction while symmetric in the y-direction. Also, $\bar{\bar{u}}_z^{(q)}$ is symmetric in both directions. In order to take advantage of these symmetry conditions along the centerlines, the global functions in Eq. (10), $\bar{\bar{u}}_i^{(q)}$, with $i = x, y, z$, are chosen as either odd or even terms of the Chebyshev polynomials in the form

$$\begin{aligned}
\bar{\bar{u}}_x^{(q)} &= \sum_{m=1,3,5,7\ldots}^{M_q+1} \sum_{n=0,2,4,6..}^{m-1} c_{xmn}^{(q)} T_m(x) T_n(y), \\
\bar{\bar{u}}_y^{(q)} &= \sum_{m=0,2,4,6\ldots}^{M_q} \sum_{n=1,3,5,7..}^{m+1} c_{ymn}^{(q)} T_m(x) T_n(y), \quad (q = s, p) \\
\bar{\bar{u}}_z^{(q)} &= \sum_{m=0,2,4,6\ldots}^{M_q} \sum_{n=0,2,4,6\ldots}^{m} c_{zmn}^{(q)} T_m(x) T_n(y).
\end{aligned} \tag{98}$$

In the skin, both in-plane and transverse displacement fields are approximated by complex potential functions of order 5 (i.e., $N_{s2} = N_{s1} = 5$) and Chebyshev polynomials of order $M_s = 24$, thus leading to a total of 321 generalized coordinates (unknowns). Due to the absence of a cutout in the patch, the

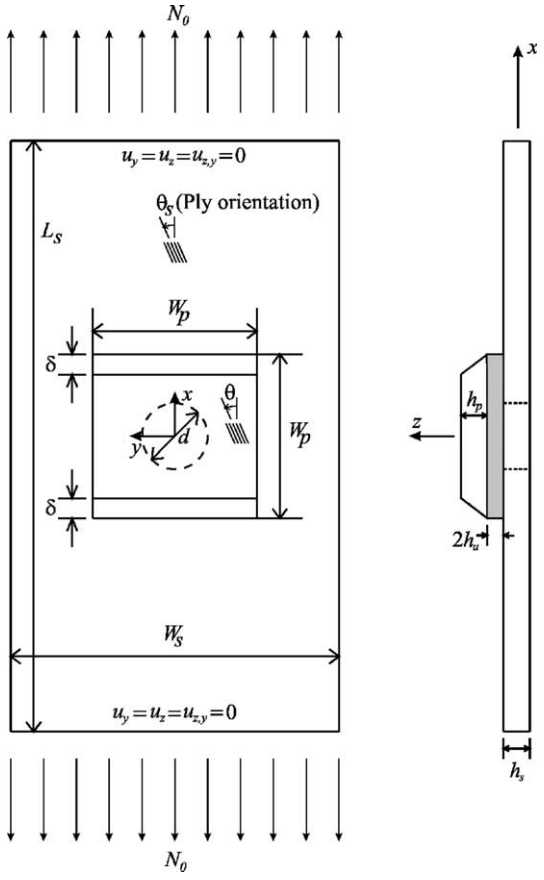

Fig. 4. Geometric parameters and loading of the skin with a circular cutout repaired by bonding a square patch.

displacement components are represented by only Chebyshev polynomials of order $M_p = 24$, (i.e., $N_{p2} = N_{p1} = 0$), thus introducing an additional 273 generalized coordinates and increasing the total number of unknowns to 638. In order to apply the clamped bending boundary conditions along the loaded edges, the reaction forces associated with the transverse deflection and the slope normal to each boundary segment are represented by 10-term Legendre polynomials, thus resulting in a total of 40 constraint equations. Additional constraint equations are also used to suppress the rigid-body motion of the skin and to ensure single-valuedness of the transverse deflection associated with the complex functions, (Madenci et al., 2001).

In both validation and demonstration cases, the skin is subjected to a uniform tension of $N_0 = 0$ to $N_0^{max} = 200$ lb/in. in 10 equal load increments along the horizontal edges, as illustrated in Fig. 4. Also, these edges are clamped in order to suppress the bending deformations. The vertical edges are free of any traction or kinematic boundary conditions. For each load step, the solution is obtained through a Newton-Raphson iteration procedure with Broyden's automatic stiffness (Jacobian) matrix update.

As shown in Fig. 4, the skin has a rectangular geometry, with its length and width specified by $L_s = 10$ in. and $W_s = 4$ in., respectively. The circular cutout at the center of the skin has a diameter of $d = 0.75$ in. The patch is square, with a length of $W_p = 1.125$ in. The thickness of the adhesive bond is specified as $2h_a = 0.0025$ in.

The Young's modulus and Poisson's ratio for aluminum are $E = 10.2 \times 10^3$ psi and $\nu = 0.33$, respectively. As shown in Fig. 2, the parameters describing the bi-linear adhesive material behavior are specified as $G_1^{(a)} = 60 \times 10^3$ psi, $G_2^{(a)} = 0.5G_1^{(a)}$, and $\gamma_c^{(a)} = 0.005$ in./in., and it has a Poisson's ratio of $\nu^{(a)} = 0.34$.

4.1. Validation

The validation is achieved for two different skin-to-patch thickness ratios. Both the skin and patch are made of aluminum. For the first case, the skin and patch have uniform thicknesses of $h_s = 0.088$ in. and $h_p = 0.024$ in., respectively, and the second case has $h_s = 0.0635$ in. and $h_p = 0.049$ in. The patch is untapered with $\delta = 0$. The comparison of the predictions against the experimental measurements presented

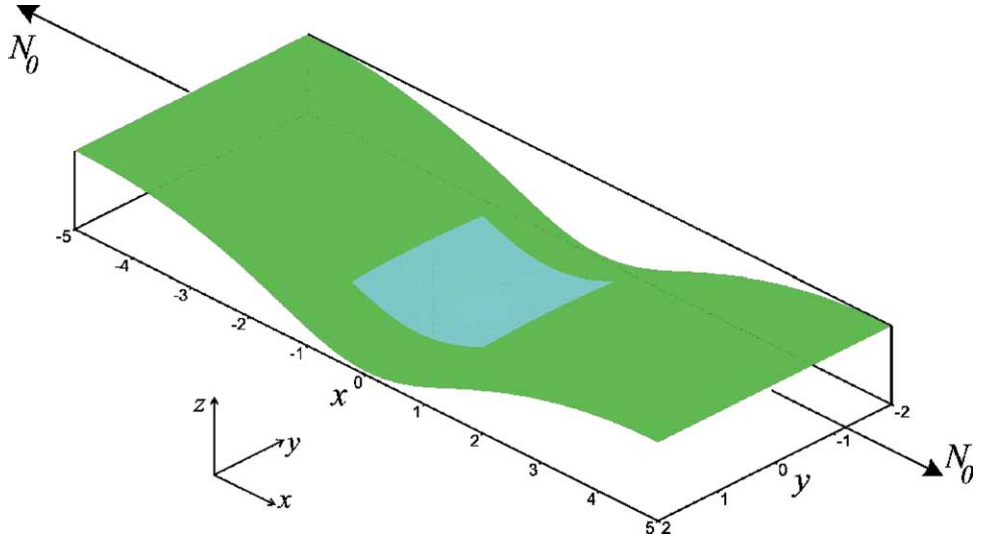

Fig. 5. A typical deformed configuration of the aluminum skin repaired by bonding an aluminum patch at a load level of $N_0/N_0^{max} = 0.5$.

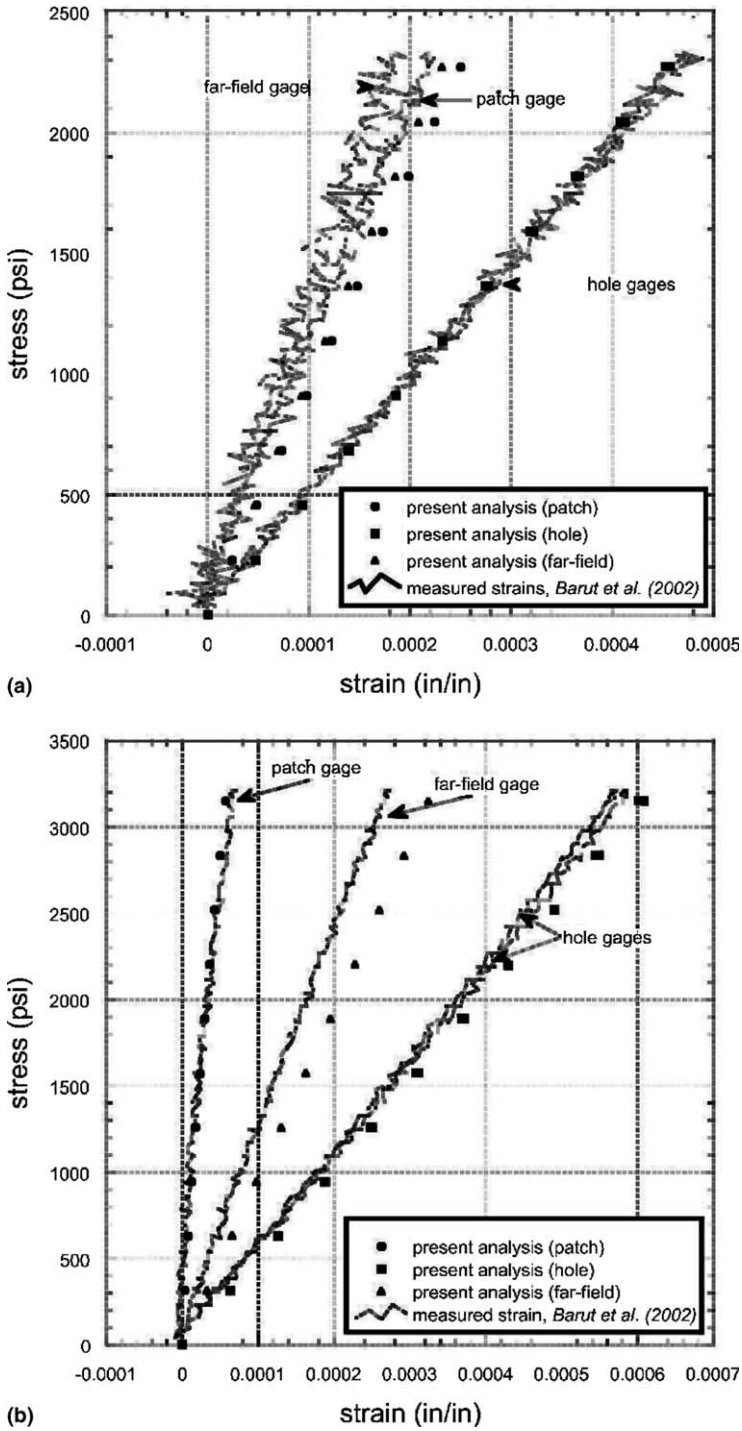

Fig. 6. Comparison of present analysis predictions against strains measured on the patch, near and away from the cutout for skin-to-patch thickness ratio: (a) 3.67 (b) 1.3.

by Barut et al. (2002) establishes the validity of the present approach. A typical deformed configuration corresponding to a load step of $N_0/N_0^{\max} = 0.5$ is shown in Fig. 5 for the aluminum skin repaired by bonding an aluminum patch. The comparison of the predicted and measured strains on the patch, near the cutout and away from the cutout on the skin shows remarkable agreement as shown in Fig. 6.

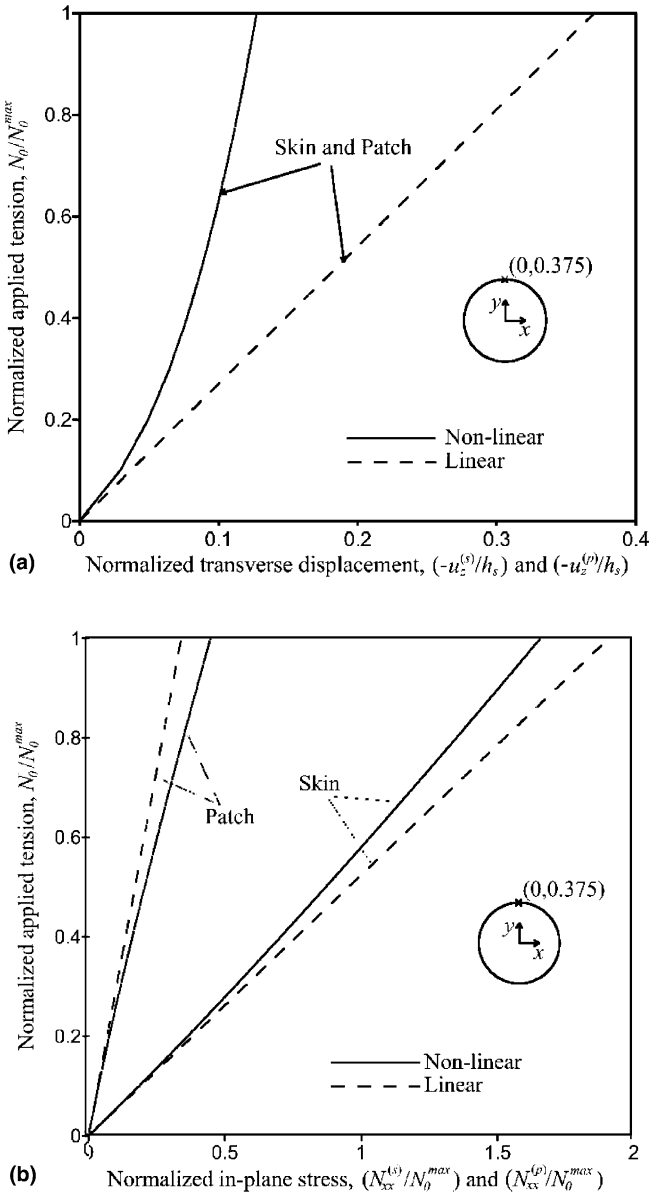

Fig. 7. The aluminum skin repaired by bonding an untapered aluminum patch at varying load levels of $N_0/N_0^{\max}$: (a) transverse displacements, $-u_z^{(s)}/h_s$ and $-u_z^{(p)}/h_s$ and (b) in-plane stress resultants, $N_{xx}^{(s)}/N_0^{\max}$ and $N_{xx}^{(p)}/N_0^{\max}$, at point $(x = 0, y = 0.35)$.

4.2. Demonstration

For the two demonstration configurations, the aluminum skin has a uniform thickness of $h_s = 0.04$ in. As shown in Fig. 4, the tapered length of the patch, denoted by δ, is varied from 0 to 0.35 in. in equal increments of 0.05 in. The thickness of the tapered patch, $h_p(x,y)$, is defined by

$$h_p(x,y) = \begin{cases} h_s(-W_p/2 + \delta \leqslant x \leqslant W_p/2 - \delta) \\ h_s - \dfrac{h_s}{\delta}(x - W_p/2 + \delta)(x \geqslant W_p/2 - \delta) \\ h_s + \dfrac{h_s}{\delta}(x + W_p/2 - \delta)(x \leqslant -W_p/2 + \delta) \end{cases} . \tag{99}$$

The quasi-isotropic composite skin has a stacking sequence of $[45/-45/0/90/90/0/-45/45]_s$. The patch is an angle-ply laminate with a stacking sequence of $[\theta/-\theta]_{2s}$, where θ varies between 0° and 90° in increments of 5°. The patch has 8 plies and its thickness is half that of the skin. The ply thickness is specified

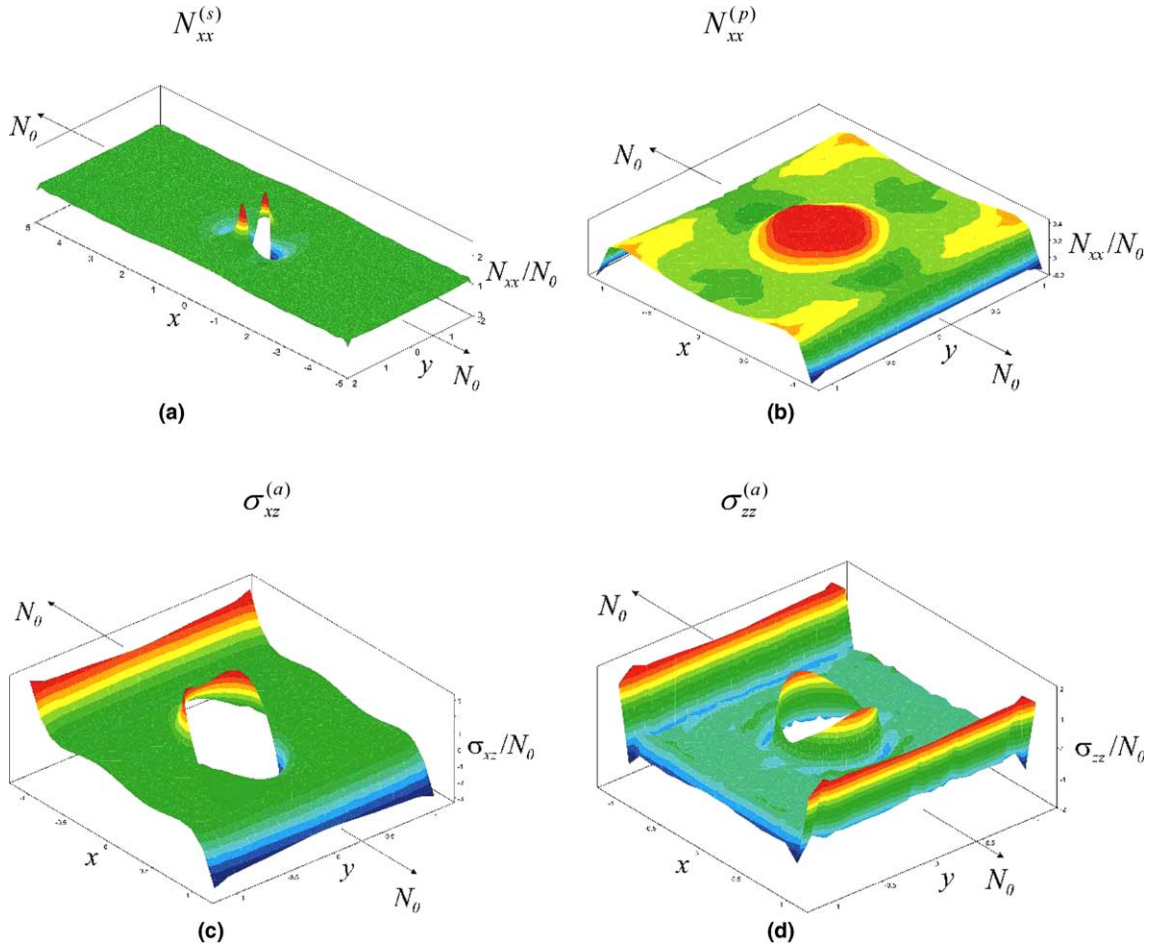

Fig. 8. Contour stresses in the aluminum skin repaired by bonding an untapered aluminum patch at a load level of $N_0/N_0^{\max} = 1$: (a) In-plane stress resultant, $N_{xx}^{(s)}$, in the skin; (b) in-plane stress resultant, $N_{xx}^{(p)}$, in the patch; (c) transverse shear stress, $\sigma_{xz}^{(a)}$, in the adhesive and (d) transverse normal stress, $\sigma_{zz}^{(a)}$, in the adhesive.

as 0.0025 in., and its material properties are specified as $E_L = 18.5 \times 10^6$ psi, $E_T = 1.64 \times 10^6$ psi, $G_{LT} = 0.87 \times 10^6$ psi, and $v_{LT} = 0.3$. The subscripts 'L' and 'T' denote the fiber and transverse directions, respectively.

4.2.1. Configuration I

The first configuration is a tapered aluminum patch bonded over a circular cutout in an aluminum skin with a linear elastic adhesive material. Corresponding to each load increment, the variation of normalized

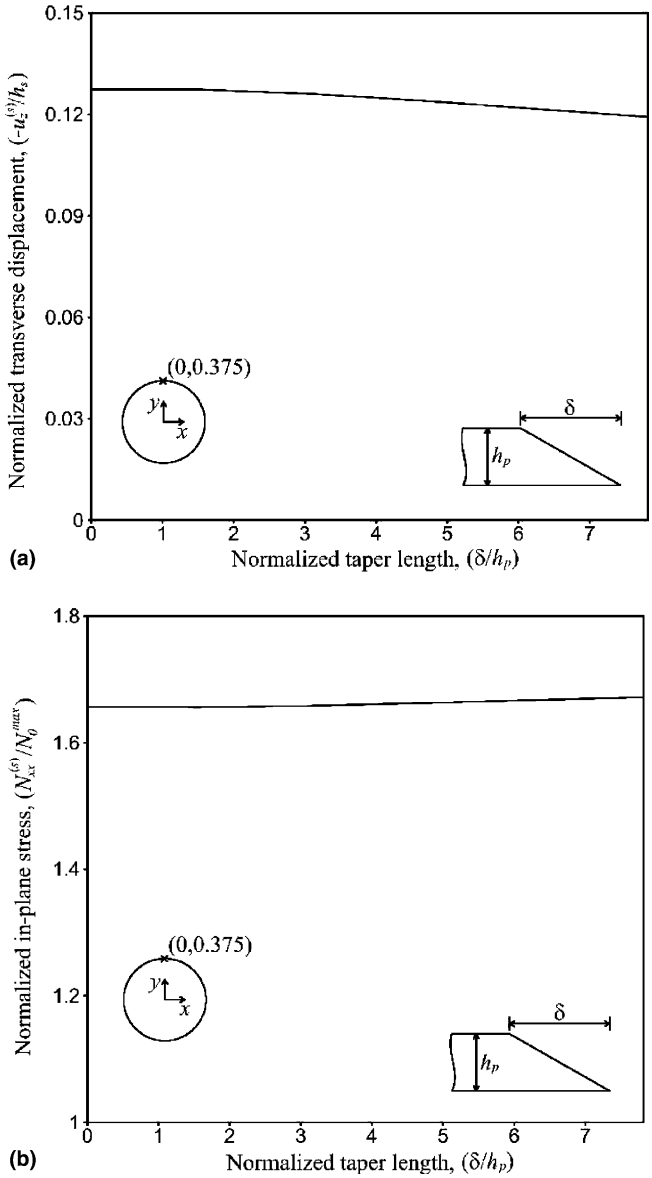

Fig. 9. The aluminum skin repaired by bonding a tapered aluminum patch at a load level of $N_0/N_0^{max} = 1$ for varying taper lengths of δ/h_p: (a) transverse displacements, $-u_z^{(s)}/h_s$ and (b) in-plane stress resultants, $N_{xx}^{(s)}/N_0^{max}$, at point $(x = 0, y = 0.35)$.

transverse displacement components in the skin and patch, $-u_z^{(s)}/h_s$ and $-u_z^{(p)}/h_s$, at the point of peak values ($x = 0$, $y = 0.375$ in.), is shown in Fig. 7a. As observed in this figure, the transverse displacements of the patch and skin are on top of each other because the peeling strains, which cause the only difference, are rather small.

As shown in Fig. 7a, the difference in transverse displacements between the linear and nonlinear analyses is significant. The magnitude of the transverse displacement obtained from the nonlinear analysis (12.5% of the skin thickness) is primarily due to the excessive stiffening of the patch and the skin arising from the applied in-plane tension. As a result, the stress stiffening of both the skin and patch tends to prevent the bending deformations arising from the eccentric in-plane loading.

For each load increment, the variations of the normalized in-plane stress resultants, $N_{xx}^{(s)}/N_0^{max}$ and $N_{xx}^{(p)}/N_0^{max}$, at the point ($x = 0$, $y = 0.375$ in.) are shown in Fig. 7b. In order to elucidate the effect of the nonlinear analysis, this figure includes the results of both the linear and nonlinear analyses. The deviation of in-plane stress resultants between the nonlinear and linear analyses is not as significant as the deviation between the nonlinear and linear transverse displacements shown in Fig. 7a. This is expected because the applied tension must be balanced by in-plane stresses in the skin and patch in order to satisfy the equilibrium of the patch-repaired skin. As shown in Fig. 7b, the nonlinear in-plane stress resultant, $N_{xx}^{(s)}$, in the skin is lower than that of the linear analysis while the nonlinear stress resultant, $N_{xx}^{(p)}$, in the patch is higher than its linear counterpart, indicating that the patch tends to compensate for any drop in the in-plane stress resultant in the skin in order to maintain equilibrium.

The three-dimensional contour plots of the in-plane stress resultant, N_{xx}, in the skin and patch at load step $N_0/N_0^{max} = 0.5$ are shown in Fig. 8a and b. As shown in these figures, the present analysis captures the stress concentrations near the circular cutout under the patch. As shown in Fig. 8a, the patch reduces the stress intensification by about 30% from the well-known stress concentration of $3N_0$. Also, the transverse shear and peeling stress distributions in the adhesive at the fifth load increment (i.e., $N_0/N_0^{max} = 0.5$) are shown in Fig. 8c and d. As shown in these figures, the present analysis captures the shearing and peeling

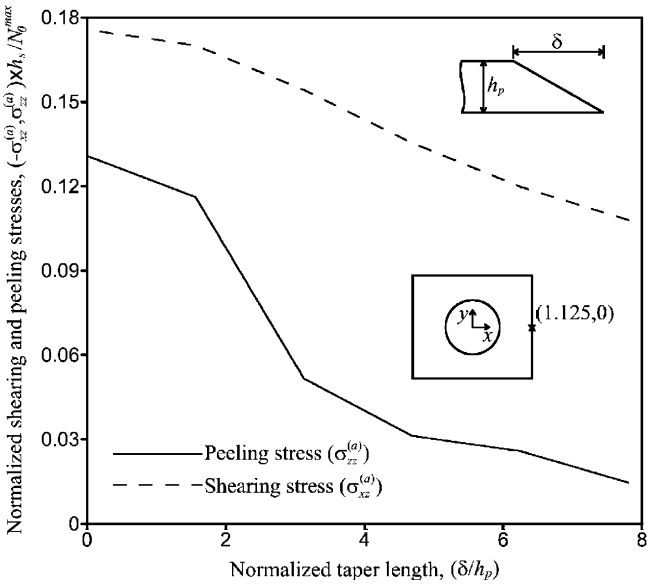

Fig. 10. The aluminum skin repaired by bonding an tapered aluminum patch at a load level of $N_0/N_0^{max} = 1$ for varying taper lengths of δ/h_p: (a) transverse shear stress, $\sigma_{xz}^{(a)}$, in the adhesive and (b) transverse normal stress, $\sigma_{zz}^{(a)}$, in the adhesive at the mid-point of the adhesive edge.

stress concentrations near the edges and the cutout, and the transverse shear stress component, $\sigma_{xz}^{(a)}$, has an asymmetric and the peeling stress, $\sigma_{zz}^{(a)}$, has a symmetric distribution. Around the hole boundary, the shear stress, $\sigma_{xz}^{(a)}$, reaches the peak values around $\pm 45°$ and $\pm 135°$. The peeling stress, $\sigma_{zz}^{(a)}$, reaches the local peak value at 90° and 270° around the hole boundary.

The effect of taper length, δ, on the out-of-plane displacement and in-plane stress components of the skin at the point ($x = 0$, $y = 0.375$) is shown in Fig. 9. The out-of-plane displacement slightly decreases with

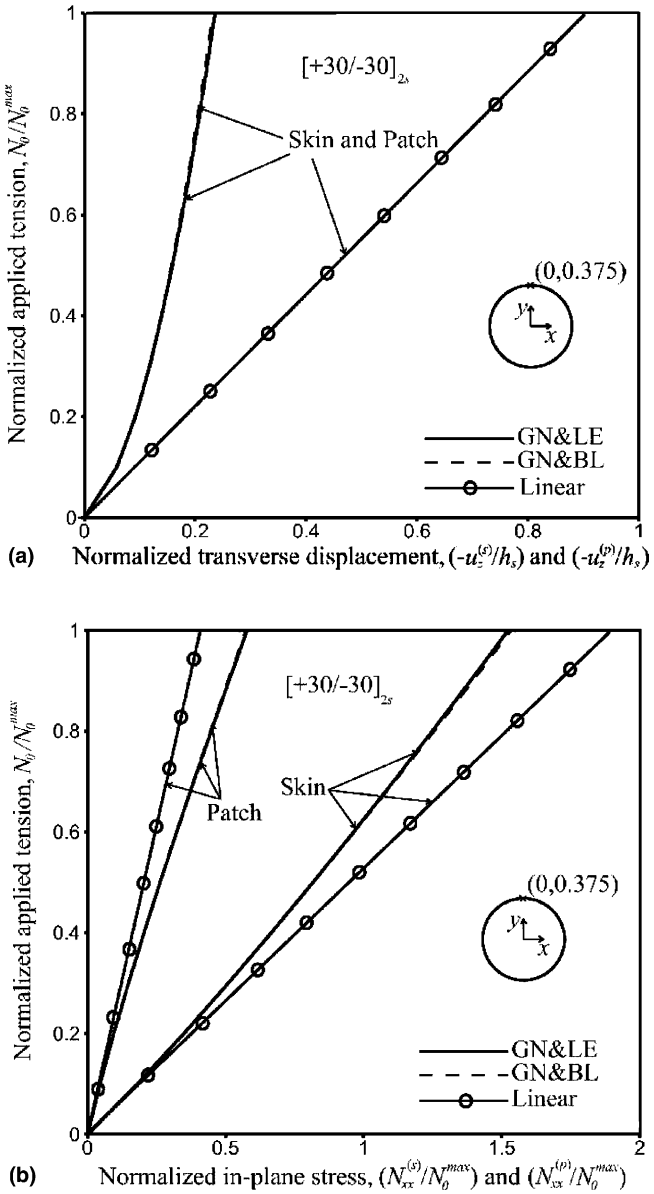

Fig. 11. The composite skin repaired by bonding an untapered composite patch at varying load levels of $N_0/N_0^{\max}$: (a) transverse displacements, $-u_z^{(s)}/h_s$ and $-u_z^{(p)}/h_s$ and (b) in-plane stress resultants, $N_{xx}^{(s)}/N_0^{\max}$ and $N_{xx}^{(p)}/N_0^{\max}$, at point ($x = 0, y = 0.35$).

increasing taper length while the normal stress component, $N_{xx}^{(s)}$, slightly increases. This behavior is expected because the increase in taper length reduces its in-plane and bending stiffnesses. This stiffness loss in the tapered patch, therefore, causes coupling between the skin and patch that is weaker than that of a skin with an untapered patch. Furthermore, the skin has to carry more load in the overlapped region in order to preserve equilibrium.

As shown in Fig. 10, the major benefit of an increasing taper length is for the reduction of the stress concentrations near the edges in the adhesive. Both the peeling and shearing stresses, evaluated at the

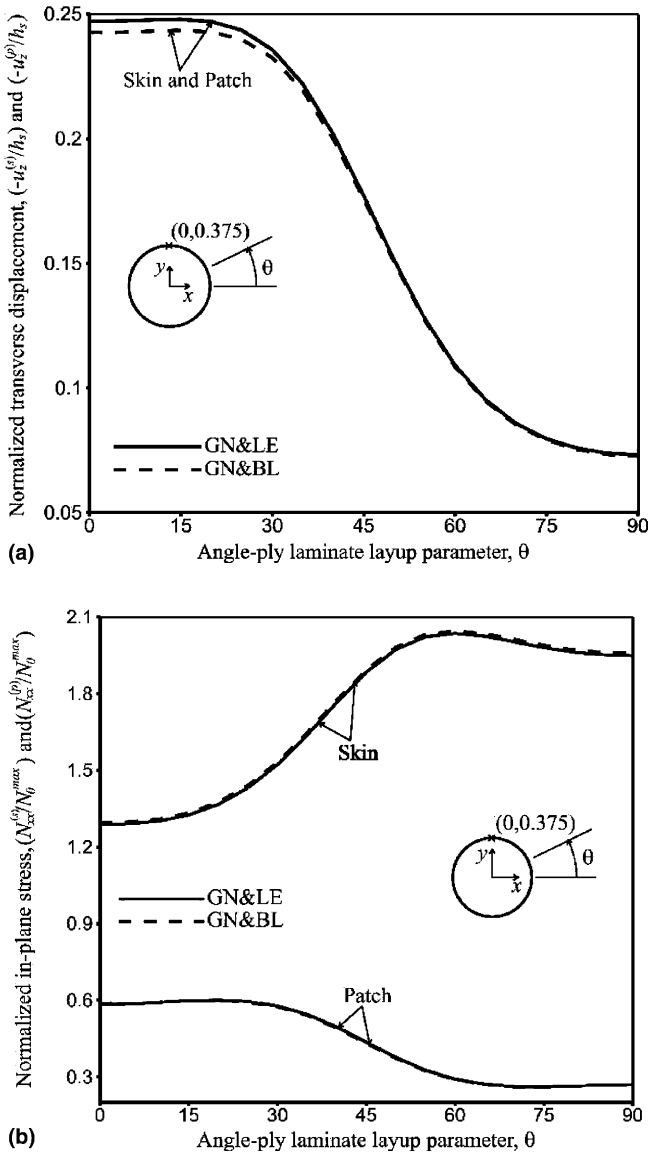

Fig. 12. The composite skin repaired by bonding an untapered composite patch at a load level of $N_0/N_0^{\max} = 1$ for a varying angle-ply layup parameter, θ: (a) transverse displacements, $-u_z^{(s)}/h_s$ and $-u_z^{(p)}/h_s$ and (b) in-plane stress resultants, $N_{xx}^{(s)}/N_0^{\max}$ and $N_{xx}^{(p)}/N_0^{\max}$, at point ($x = 0$, $y = 0.35$).

mid-point of the edges perpendicular to the loading direction, reduce considerably with increasing taper length. The reduction in shearing stress is more significant than that of the peeling stress in comparison to that of the untapered patch.

4.2.2. Configuration II

The second configuration is an untapered composite patch bonded over a circular cutout in a composite skin with a bi-linear elastic adhesive material. For a 30° angle-ply patch layup and a quasi-isotropic skin, the variation of the normalized out-of-plane displacement, u_z, and the normalized in-plane stress, $N_{xx}/N_0^{\max}$, evaluated at point ($x = 0$, $y = 0.375$) under increasing uniform tension is shown in Figs. 11a,b. In these figures, the dashed and solid lines denote the geometrically nonlinear analyses with bi-linear (GN and BL) and linear (GN and LE) adhesive material behavior. The solid line with hollow circles denote the geometrically linear analysis results with linearly elastic adhesive material properties.

As observed in Fig. 11a, the stiffening effect due to in-plane loading has a significant effect on reducing the out-of-plane displacement of both the patch and the skin. The stiffening effect arising from the nonlinear strain measure reduces the deflections by almost two-thirds that of the linear analysis. Furthermore, there is a considerable difference in the in-plane stress resultants, $N_{xx}/N_0^{\max}$, between the linear and geometrically nonlinear analyses, as observed in Fig. 11b. However, the decrease in the in-plane stress resultant in the skin due to geometrically nonlinear effects is compensated for by an increase in the patch.

The effect of angle-ply patch layup on the out-of-plane displacement and in-plane stress components is captured in Figs. 12a,b. Both the in-plane displacement and in-plane stress resultant components are evaluated at point ($x = 0$, $y = 0.375$). As shown in Fig. 12a, the out-of-plane displacements of both the skin and patch reduce as the patch layup parameter, θ, changes from 0° to 90°. It reaches the maximum at the 0° angle-ply layup and becomes minimum at the 90 angle-ply layup. This figure also indicates that the coupling between the skin and patch decreases as the in-plane and bending stiffnesses of the patch

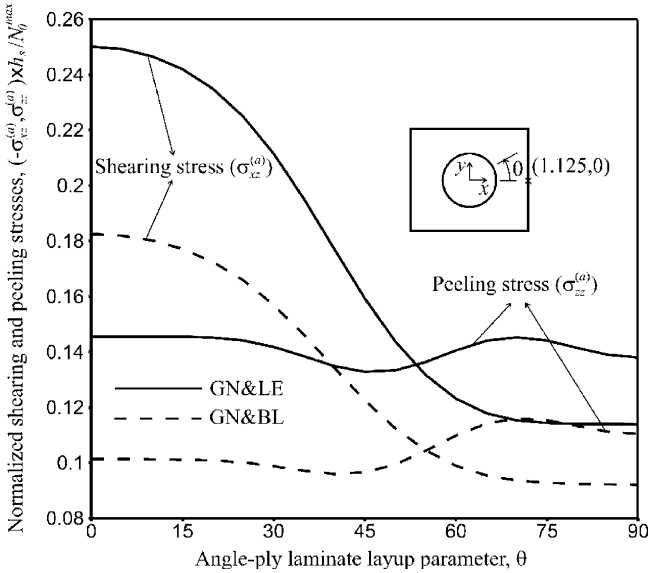

Fig. 13. The composite skin repaired by bonding an untapered composite patch at a load level of $N_0/N_0^{\max} = 1$ for a varying angle-ply layup parameter, θ: (a) transverse shear stress, $\sigma_{xz}^{(a)}$, in the adhesive and (b) transverse normal stress, $\sigma_{zz}^{(a)}$, in the adhesive at the mid-point ($x = 0$, $y = 0.35$) of the adhesive edge.

decreases in the loading direction. Shown in Fig. 12b, this effect is also apparent by the behavior of the skin. It tends to carry more in-plane load as the in-plane stiffness of the patch becomes weaker in the loading direction.

Although the bi-linear material behavior of the adhesive has an insignificant effect on the overall response of the patch and skin, its effect on the response of adhesive stresses along the edges of the adhesive is considerable, as shown in Fig. 13. Also, the change in the angle-ply patch layup parameter, θ, reduces the shearing stresses considerably while influencing the peeling stress slightly.

As shown in Fig. 14, the influence of the bi-linear material response on the effective shearing strain in the adhesive is illustrated through four load steps of $N_0/N_0^{\max} = 0.3, 0.5, 0.8, 1.0$. In this figure, the light and dark areas represent the regions where the effective shearing strains are, respectively, below and above the characteristic value of $\gamma_c^{(a)}$. As expected, the shearing strains start to exceed the critical value at the corners and near the cutout in the adhesive first and then grow towards the interior of the adhesive domain as the applied load increases.

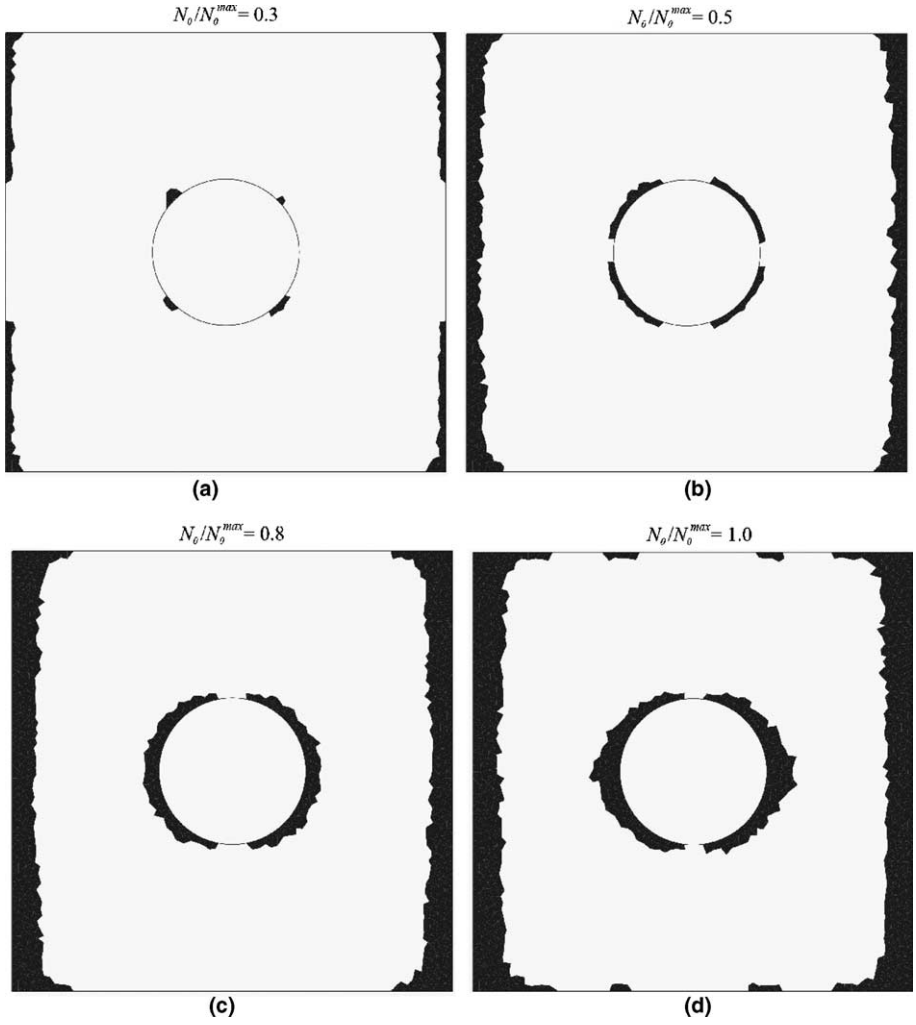

Fig. 14. Distribution of effective shear strain in the adhesive at load steps of $N_0/N_0^{\max} = 0.3, 0.5, 0.8, 1.0$.

5. Conclusions

A geometrically nonlinear analytical approach for determining the stress and displacement fields in a bonded patch-repaired skin with a circular cutout is presented. This approach accounts for the presence of tapered patch geometry and stacking sequence, as well as the linear and bi-linear elastic material behaviors. It captures the in-plane stress concentrations near the cutout and the stress concentrations in both transverse shear and peeling stresses near the corners while including the stiffening effects in both the skin and patch arising from in-plane tensile loading.

The stiffening of both the skin and patch significantly reduces the out-of-plane displacement. Although noticeable, the effect of geometric nonlinearity on the in-plane stress response of both the patch and skin is not considerably large. Any decrease in the in-plane stress distribution in the skin causes an increase in the in-plane stress distribution in the patch.

The tapered patch geometry slightly changes the response of the patch and the skin but considerably reduces the peeling and shearing stress concentrations near the edges of the adhesive. As the angle-ply parameter, θ, of the patch layup increases, the in-plane and the bending stiffnesses of the patch decrease in the loading direction. Therefore, the skin carries more load, thus experiences higher in-plane stresses. Therefore, as the angle-ply parameter, θ, of the patch layup increases, the skin carries more load and experiences higher in-plane stresses because of the reduction of the in-plane and bending patch stiffnesses in the loading direction.

Also, the coupling between the skin and patch is reduced due to the stiffness loss of the patch in the loading direction. As a result, the out-of-plane displacements of both the skin and patch decrease as the angle-ply layup parameter increases. In the adhesive, the increase in this parameter mainly reduces the shearing stresses and slightly changes the peeling stresses.

The bi-linear adhesive material behavior has almost no effect on the overall behavior of the patch and skin. In the adhesive, however, both shearing and peeling stresses reduce considerably in the areas where the shearing strains go beyond the characteristic value of the bi-linear behavior.

Appendix A

The complex potential functions, $\mathbf{\Phi}_{nk}^{(q)}(z_{\varepsilon k}^{(q)})$ with $q = \mathrm{s,p}$, appearing in Eq. (8) are defined as

$$\mathbf{\Phi}_{nk}^{(\mathrm{s})}(z_{\varepsilon k}^{(\mathrm{s})}) = (\xi_{\varepsilon k}^{(\mathrm{s})})^n, \tag{A.1a}$$

$$\mathbf{\Phi}_{nk}^{(\mathrm{p})}(z_{\varepsilon k}^{(\mathrm{p})}) = (z_{\varepsilon k}^{(\mathrm{p})})^n. \tag{A.1b}$$

The mapping functions $\xi_{\varepsilon k}^{(\mathrm{s})}$, first introduced by Bowie (1956), map a cutout onto a unit circle. In this analysis, the mapping functions for an elliptical cutout, introduced by Lekhnitskii (1968), are employed in the form

$$\xi_{\varepsilon k}^{(\mathrm{s})} = \frac{z_{\varepsilon k}^{(\mathrm{s})} \pm \sqrt{\left(z_{\varepsilon k}^{(\mathrm{s})}\right)^2 - a^2 - \left(\mu_{\varepsilon k}^{(\mathrm{s})}\right)^2 b^2}}{a - I\left(\mu_{\varepsilon k}^{(\mathrm{s})}\right)^2 b} \quad (k = 1, 2) \tag{A.2}$$

in which $z_{\varepsilon k}^{(q)} = x_q + \mu_{\varepsilon k}^{(q)} y_q (q = s, p)$ and a and b are the major and minor axes of the elliptical cutout, with $I = \sqrt{-1}$. The sign of the square root term is chosen so that $|\ \xi_{\varepsilon k}^{(\mathrm{s})}\ | 1$.

Inverting the mapping function provides $\omega_{\varepsilon k}^{(\mathrm{s})}(\xi_{\varepsilon k}^{(\mathrm{s})})$ as

$$z_{\varepsilon k}^{(\mathrm{s})} = \omega_{\varepsilon k}^{(\mathrm{s})}\left(\xi_{\varepsilon k}^{(\mathrm{s})}\right) = r_{\varepsilon k}\xi_{\varepsilon k}^{(\mathrm{s})} - \frac{s_{\varepsilon k}}{\xi_{\varepsilon k}^{(\mathrm{s})}} \tag{A.3}$$

in which

$$r_{\varepsilon k} = \frac{1}{2}(a - I\mu_{\varepsilon k}^{(s)} b), \quad s_{\varepsilon k} = \frac{1}{2}(a + I\mu_{\varepsilon k}^{(s)} b). \tag{A.4}$$

The unknown complex constants, $\mu_{\varepsilon 1}^{(q)}$ and $\mu_{\varepsilon 2}^{(q)} (q = s, p)$, and their complex conjugates, i.e., $\mu_{\varepsilon 3}^{(q)} = \bar{\mu}_{\varepsilon 3}^{(q)}$ and $\mu_{\varepsilon 4}^{(q)} = \bar{\mu}_{\varepsilon 2}^{(q)}$, are the roots of the characteristic equation obtained from the in-plane compatibility condition

$$a_{11}'^{(q)} \left(\mu_{\varepsilon k}^{(q)}\right)^4 - 2a_{16}'^{(q)} \left(\mu_{\varepsilon k}^{(q)}\right)^3 + \left(2a_{26}'^{(q)} + a_{66}'^{(q)}\right) \left(\mu_{\varepsilon k}^{(q)}\right)^2 - 2a_{26}'^{(q)} \mu_{\varepsilon k}^{(q)} + a_{22}'^{(q)} = 0 \tag{A.5}$$

in which the coefficients $a_{ij}'^{(q)}$ are components of the flexibility matrix $\mathbf{a}'^{(q)}$, which is the inverse of the in-plane stiffness matrix, $\mathbf{A}'^{(q)}$. Both the flexibility and the stiffness matrices, $\mathbf{a}'^{(q)}$ and $A'^{(q)}$, are measured with respect to the local coordinate system (x_q, y_q). The angle $\psi^{(q)}$ represents the orientation of the local coordinate system with respect to the global coordinate system. Thus, the components of $\mathbf{A}'^{(q)}$ can be directly obtained by transforming the components of the in-plane stiffness matrix, $\mathbf{A}^{(q)}$, defined in the global system through the orientation angle. This transformation relation is available in any textbook on composite materials. Also, the complex constants, $p_k^{(q)}$ and $q_k^{(q)}$, in Eq. (9) are defined as

$$p_k^{(q)} = a_{11}'^{(q)} (\mu_{\varepsilon k}^{(q)})^2 + a_{12}'^{(q)} - a_{16}'^{(q)} \mu_{\varepsilon k}^{(q)}, \tag{A.6a}$$

$$q_k^{(q)} = a_{12}'^{(q)} \mu_{\varepsilon k}^{(q)} + a_{22}'^{(q)} / \mu_{\varepsilon k}^{(q)} - a_{26}'^{(q)}. \tag{A.6b}$$

The complex functions, $\mathbf{F}_{nk}^{(s)}(z_{\kappa k}^{(s)})$, appearing in the expression for the local functions, $\bar{u}_z^{(q)}$, with $q = \mathrm{s}, \mathrm{p}$, in (8c) are defined as

$$\mathbf{F}_{nk}^{(s)}(z_{\kappa k}^{(s)}) = \begin{cases} \dfrac{r_{\kappa k}}{n} (\xi_{\kappa k}^{(s)})^n - \dfrac{s_{\kappa k}}{n-2} (\xi_{\kappa k}^{(s)})^{n-2}, & n \geqslant 3 \\ \dfrac{r_{\kappa k} (\xi_{\kappa k}^{(s)})^2}{2} - s_{\kappa k} \ln \xi_{\kappa k}^{(s)}, & n = 2 \\ (z_{\kappa k}^{(s)})^n, & n = 0, 1, \\ r_{\kappa k} \ln \xi_{\kappa k}^{(s)} + \dfrac{s_{\kappa k} (\xi_{\kappa k}^{(s)})^{-2}}{2}, & n = -1 \\ \dfrac{r_{\kappa k}}{n+1} (\xi_{\kappa k}^{(s)})^{n+1} - \dfrac{s_{\kappa k}}{n-1} (\xi_{\kappa k}^{(s)})^{n-1}, & n \leqslant -2 \end{cases} \tag{A.7a}$$

$$\mathbf{F}_{nk}^{(p)}(z_{\kappa k}^{(p)}) = (z_{\kappa k}^{(p)})^n \quad \text{with } n \geqslant 0 \tag{A.7b}$$

in which the expressions for the mapping function, $\xi_{\kappa k}^{(p)}$, and the constants, $r_{\kappa k}$ and $s_{\kappa k}$, are respectively, in the same form as the expressions for $\xi_{\varepsilon k}^{(s)}$, $r_{\varepsilon k}$, and $s_{\varepsilon k}$, except that the subscript ε is replaced by κ.

In Eq. (A.7a,b), the complex variables $z_{\kappa k}^{(q)}$, with $q = \mathrm{s}, \mathrm{p}$, are defined in the form

$$z_{\kappa k}^{(q)} = x_q + \mu_{\kappa k}^{(q)} y_q \tag{A.8}$$

in which the unknown complex constants, $\mu_{\kappa 1}^{(q)}$ and $\mu_{\kappa 2}^{(q)}$, and their conjugates are obtained from the bending equilibrium equations for an unpatched plate

$$D_{22}'^{(q)} (\mu_{\kappa k}^{(q)})^4 + 4D_{26}'^{(q)} (\mu_{\kappa k}^{(q)})^3 + (2D_{12}'^{(q)} + 4D_{66}'^{(q)}) (\mu_{\kappa k}^{(q)})^2 + 4D_{16}'^{(q)} \mu_{\kappa k}^{(q)} + D_{11}'^{(q)} = 0, \tag{A.9}$$

where $D_{ij}'^{(q)}$ are the components of the bending stiffness matrix $\mathbf{D}'^{(q)}$, which is defined with respect to the local coordinate system (x_q, y_q). The bending stiffness matrix, $D'^{(q)}$, can be directly obtained from the transformation of matrix $\mathbf{D}^{(q)}$ defined in the global coordinates. This transformation relation is available in any textbook on composite materials.

The local vector of complex interpolation functions, $\overline{\mathbf{V}}_{\alpha}^{(q)}$ ($\alpha = x, y, z$), appearing in Eq. (11) are defined as

$$\overline{\mathbf{V}}_{\alpha}^{(q)^{\mathrm{T}}} = \left\{ \overline{\mathbf{V}}_{\alpha(N_{q1})}^{(q)^{\mathrm{T}}}, \quad \overline{\mathbf{V}}_{\alpha(N_{q1}-1)}^{(q)^{\mathrm{T}}}, \quad \ldots, \quad \overline{\mathbf{V}}_{\alpha n}^{(q)^{\mathrm{T}}}, \quad \ldots, \quad \overline{\mathbf{V}}_{\alpha(N_{q2})}^{(q)^{\mathrm{T}}} \right\} \tag{A.10}$$

with

$$\overline{\mathbf{V}}_{\alpha(n)}^{(q)^{\mathrm{T}}} = \left\{ \overline{\mathbf{V}}_{\alpha(n1)}^{(q)^{\mathrm{T}}}, \overline{\mathbf{V}}_{\alpha(n2)}^{(q)^{\mathrm{T}}} \right\} \quad (q = \mathrm{s}, \mathrm{p}; \alpha = x, y) \tag{A.11}$$

in which

$$\overline{\mathbf{V}}_{\alpha(nk)}^{(q)^{\mathrm{T}}} = \left\{ 2\mathrm{Re}\left[d_{\alpha k}^{(q)} \mathbf{\Phi}_{nk}^{(q)} \right], -2\mathrm{Im}\left[d_{\alpha k}^{(q)} \mathbf{\Phi}_{nk}^{(q)} \right] \right\} \quad (q = \mathrm{s}, \mathrm{p}; \alpha = x, y; k = 1, 2) \tag{A.12}$$

and

$$\overline{\mathbf{V}}_{z}^{(q)^{\mathrm{T}}} = \left\{ \overline{\mathbf{V}}_{z(N_{q1})}^{(q)^{\mathrm{T}}}, \quad \overline{\mathbf{V}}_{z(N_{q1}-1)}^{(q)^{\mathrm{T}}}, \quad \ldots, \quad \overline{\mathbf{V}}_{z(n)}^{(q)^{\mathrm{T}}}, \quad \ldots, \quad \overline{\mathbf{V}}_{z(N_{q2})}^{(q)^{\mathrm{T}}} \right\} \tag{A.13}$$

with

$$\overline{\mathbf{V}}_{z(n)}^{(q)^{\mathrm{T}}} = \left\{ \overline{\mathbf{V}}_{z(n1)}^{(q)^{\mathrm{T}}}, \quad \overline{\mathbf{V}}_{z(n2)}^{(q)^{\mathrm{T}}} \right\} \quad (q = s, p) \tag{A.14}$$

in which

$$\overline{\mathbf{V}}_{z(nk)}^{(q)^{\mathrm{T}}} = \left\{ 2\mathrm{Re}\left[F_{nk}^{(q)} \right], -2\mathrm{Im}\left[F_{nk}^{(q)} \right] \right\} \quad (q = \mathrm{s}, \mathrm{p}; k = 1, 2). \tag{A.15}$$

The corresponding vectors of unknown coefficients, $\alpha^{(q)}$ and $\boldsymbol{\beta}^{(q)}$, are defined in the form

$$\boldsymbol{\alpha}^{(q)^{\mathrm{T}}} = \left\{ \boldsymbol{\alpha}_{N_{q1}}^{(q)^{\mathrm{T}}}, \quad \boldsymbol{\alpha}_{N_{q1}+1}^{(q)^{\mathrm{T}}}, \quad \ldots, \quad \boldsymbol{\alpha}_{n}^{(q)^{\mathrm{T}}}, \quad \ldots, \quad \alpha_{N_{q2}}^{(q)^{\mathrm{T}}} \right\} \tag{A.16}$$

in which

$$\alpha_{n}^{(q)^{\mathrm{T}}} = \left\{ \alpha_{n1}^{(q)^{\mathrm{T}}}, \quad \alpha_{n2}^{(q)^{\mathrm{T}}} \right\} \tag{A.17}$$

with

$$\alpha_{nk}^{(q)^{\mathrm{T}}} = \left\{ \mathrm{Re}\left[\alpha_{nk}^{(q)} \right], \quad \mathrm{Im}\left[\alpha_{nk}^{(q)} \right] \right\} \tag{A.18}$$

and

$$\boldsymbol{\beta}^{(q)^{\mathrm{T}}} = \left\{ \boldsymbol{\beta}_{N_{q1}}^{(q)^{\mathrm{T}}}, \quad \beta_{N_{q1}+1}^{(q)^{\mathrm{T}}}, \quad \ldots, \quad \beta_{n}^{(q)^{\mathrm{T}}}, \quad \ldots, \quad \beta_{N_{q2}}^{(q)^{\mathrm{T}}} \right\} \tag{A.19}$$

in which

$$\boldsymbol{\beta}_{n}^{(q)^{\mathrm{T}}} = \left\{ \boldsymbol{\beta}_{n1}^{(q)^{\mathrm{T}}}, \quad \boldsymbol{\beta}_{n2}^{(q)^{\mathrm{T}}} \right\} \tag{A.20}$$

with

$$\boldsymbol{\beta}_{nk}^{(q)^{\mathrm{T}}} = \left\{ \mathrm{Re}\left[\boldsymbol{\beta}_{nk}^{(q)} \right], \quad \mathrm{Im}\left[\boldsymbol{\beta}_{nk}^{(q)} \right] \right\}. \tag{A.21}$$

Also, the vector of global interpolation functions, $\overline{\overline{\mathbf{V}}}_{\alpha}^{(q)}$ ($\alpha = x, y, z$), and their associated unknown vectors, $\mathbf{c}_{\alpha}^{(q)}$, in Eq. (11a,b) are defined as

$$\overline{\overline{\mathbf{V}}}_{\alpha}^{(q)^{\mathrm{T}}} = \{T_{00}(x,y), \quad T_{10}(x,y), \quad T_{01}(x,y), \quad T_{20}(x,y), \quad T_{11}(x,y), \; T_{02}(x,y), \quad \ldots, \quad T_{0M_q}(x,y)\} \tag{A.22}$$

in which $T_{ij}(x,y) = T_i(x)T_j(y)$ and

$$\mathbf{c}_{\alpha}^{\mathrm{T}} = \{\, c_{\alpha 00}, \quad c_{\alpha 10}, \quad c_{\alpha 01}, \quad c_{\alpha 20}, \quad c_{\alpha 11}, \quad c_{\alpha 02}, \quad \ldots, \quad c_{\alpha 0M_q} \,\}. \tag{A.23}$$

References

Andruet, R.H., Dillard, D.A., Holzer, S.M., 2001. Two- and three-dimensional geometrically nonlinear finite element analysis of adhesive joints. Int. J. Adhesion Adhesives 21, 17–34.

Barut, A., Hanauska, J., Madenci, E., Ambur, D.A., 2002. Analysis method for bonded patch repair of a skin with a cutout. Compos. Struct. 55, 277–294.

Bowie, O.L., 1956. Analysis of an infinite plate containing radial cracks originating at the boundary of an internal circular hole. J. Math. Phys. 35, 60–71.

Duong, C.N., Yu, J., 2003. Thermal stresses in one-sided bond repair: geometrically nonlinear analysis. Theor. Appl. Fract. Mech. 40, 197–209.

Fung, Y.C., Tong, P., 2001. Classical and Computational Solid Mechanics. World Scientific Publishing Co. Pte. Ltd., Singapore.

Geradin, M., Idelson, S., Hoggie, M., 1981. Computational strategies for the solution of large nonlinear problems via quasi-Newton methods. Comput. Struct. 13, 73–81.

Klug, J.C., Sun, C.T., 1998. Large deflection effects of cracked aluminum plates repaired with bonded composite patches. Compos. Struct. 42, 291–296.

Lekhnitskii, S.G., 1968. Anisotropic Plates. Gordon and Breach Science Publishers, Inc., New York.

Madenci, E., Barut, A., Nemeth, M.P., 2001. A complex potential-variational method for stress analysis of unsymmetric laminates with an inclined cutout. ASME J. Appl. Mech. 68, 731–739.

Naboulsi, S., Mall, S., 1998. Nonlinear analysis of bonded composite patch repair of cracked aluminum panels. Compos. Struct. 41, 303–313.

Tong, L., Xiannian, S., 2003. Nonlinear stress analysis for bonded patch to curved thin-walled structures. Int. J. Adhesion Adhesives 23, 349–364.

Washizu, K., 1982. Variational Methods in Elasticity and Plasticity. Pergamon Press Inc., New York.